



DARK MATTER FREEZE-IN FROM
NON-EQUILIBRIUM QUANTUM FIELD THEORY:
TREATMENT OF REAL INTERMEDIATE STATES

MASTER THESIS

Jan Ravi Bade

Universität Münster

Institut für theoretische Physik

AG Klasen

Supervisor: Prof. Dr. Michael Klasen

Second examiner: Prof. Dr. Marco Drewes

Münster, June 2025

Declaration of Academic Integrity

I hereby confirm that this thesis on the

“Dark Matter Freeze-in from Non-equilibrium Quantum Field Theory: Treatment of Real Intermediate States”

is solely my own work and that I have used no sources or aids other than the ones stated. All passages in my thesis for which other sources, including electronic media, have been used, be it direct quotes or content references, have been acknowledged as such and the sources cited. I agree to have my thesis checked in order to rule out potential similarities with other works and to have my thesis stored in a database for this purpose.

I certify that I have not submitted this thesis or parts of it elsewhere as an examination paper.

Münster, June 19, 2025

Signature

Acknowledgement

First of all, I would like to thank my research group and Prof. Michael Klasen, as well as the members of my office for a friendly environment. I want to especially thank Luca for providing the topic of this thesis, answering many questions and some code examples, as well as Adrian with whom I had countless discussions about thermal field theory. I would also like to thank Justus, who provided plenty of advice for efficient calculations on PALMA.

I am very grateful for the many friends I have made throughout my studies, who provided a constant source of companionship and encouragement. I would also like to thank all those, who read parts of this thesis and provided useful commentary: Daniel, Katrin, Jan, Jannis, Adrian and Jonah. I would also like to thank my parents for constantly supporting me and finding countless comma errors in my thesis, despite not understanding much of the content.

I should point out, that parts of the calculations for this thesis were performed on the HPC cluster PALMA II of the University of Münster, subsidised by the DFG (INST 211/667-1).

Contents

1	Introduction	1
2	Dark Matter freeze-in in the Boltzmann equation formalism	5
2.1	Dark Matter	5
2.1.1	Indications of the existence of Dark Matter	5
2.1.2	Dark matter candidates	7
2.2	Freeze-in of FIMP dark matter	8
2.3	Scalar singlet dark matter model	10
2.4	Relic density calculations in the Boltzmann equation formalism	11
2.5	Scattering terms in the Boltzmann equation	15
2.6	Relevant decay rates for Boltzmann-processes	20
2.7	Relevant $2 \rightarrow 2$ cross sections	21
2.8	Real Intermediate State problem	26
3	Dark Matter freeze-in in non-equilibrium field theory	31
3.1	FTFT formalisms	32
3.2	Introduction to the time path formalism	32
3.2.1	Equilibrium propagators in the CTP formalism	36
3.2.2	The Dyson-Schwinger and Kadanoff-Baym equations	40
3.3	From the Kadanoff-Baym equations to a time evolution of the DM density	42
3.4	Dark matter self energy	45
3.5	Thermal Higgs self energies	47
3.5.1	Wightmann self energy	47
3.5.2	Hermitian self energy	51
3.6	DM Production from multiple orders	53
3.6.1	Decay terms from bare propagators	54
3.6.2	1-loop self energy and $2 \rightarrow 2$ scattering	55
3.6.3	Cancellation of the pinch singularities and additional finite contributions	57
3.7	Temperature dependent Higgs potential	58
4	Numerical results	65
4.1	Comparing the impact of different particle species	65
4.2	CTP calculations and different RIS schemes	65

4.3	Impact of the temperature dependent Higgs potential	67
5	Conclusion	69
6	Outlook	69
A	Notes about the numerical implementation	71
A.1	Solving the semi-classical Boltzmann equation in Python	71
A.2	FTFT calculations in C	72
A.3	Calculation of the Higgs VEV and mass in Python	72
B	Higgs potential in high temperature approximation	73
	Bibliography	75

1 Introduction

The standard model of cosmology, Λ CDM, has proven to be very successful in explaining many observations of our universe [1, 2]. It allows for a consistent explanation of both the cosmic microwave background (CMB) [3] as well as large scale structure observations [4]. However, it requires the existence of an additional matter component, which is not explained by the standard model (SM) of particle physics, the so-called dark matter. Despite the continued search for dark matter, there still has not been any direct detection. Therefore, we know very little about the dark matter in our universe and many different theories of dark matter are possible.[5]

What we do, however, know about dark matter, is its abundance in the universe. Examinations of the cosmic microwave background (CMB) yield strict constraints on the dark matter relic density in our universe [3]. One of the key requirements of dark matter models is therefore, whether they can explain the currently observed dark matter relic density. Consequently, in order to analyse dark matter models, it is important to be able to perform reliable and precise calculations of the relic density.

The standard tool for relic density calculations is the semi-classical Boltzmann equation using transition probabilities calculated in zero temperature QFT [6]. The most studied dark matter models rely on freeze-out scenarios [7, 8, 9]. Here, the relevant dynamics take place after the freeze-out of dark matter at low temperatures. Therefore, the calculations are performed at low temperature and the use of zero temperature QFT is well justified. However, high temperature effects can be relevant beyond freeze-out scenarios[10]. The semi-classical Boltzmann equations as described above, struggle to account for the high temperature dynamics in these cases.

Additionally, when s -channel processes determine the dynamics and real intermediate states (RIS) are kinematically allowed, the semi-classical Boltzmann equations will exhibit a double counting of decay terms. This is a well known problem and many different schemes to eliminate this double counting have been discussed in the past [11, 12]. There is a priori no unique correct way of treating the RIS problem, and further problems appear in scenarios where multiple channels may mix.

Alternatively, relic densities can be calculated directly from self energies in the closed time

path formulation of non-equilibrium field theory [13, 14]. This both naturally encompasses certain temperature dependent effects and circumvents the RIS problem when resummed propagators are used.

Non-equilibrium or finite temperature field theories (FTFTs) are quantum field theories which naturally include the effects that a medium or a high temperature background may have on particles. FTFTs have been developed since the 1950s. While first applications were in many body physics [15], FTFTs have gained relevance in the particle physics community to examine such fields as the quark-gluon plasma [16, 17, 18], neutrino physics [19, 20], or dark matter physics [13].

Additionally, FTFTs are well suited to analyze phase transitions and the temperature dependent evolution of related potentials [21]. This is relevant in Higgs physics [22], but also for example for phase transitions in the early universe which can be relevant in the explanation of gravitational wave signals [23]. The temperature dependence of cosmological potentials can also be relevant in dark matter relic density calculations. As noted above, high temperature regimes may be relevant for dark matter production and the modified potentials may greatly affect the dynamics of the related particles.

In this thesis, we test and compare the impact of the above mentioned methods by applying them to the freeze-in of scalar singlet dark matter (SSDM)[24]. While the procedure in the CTP formalism is similar to [13], here we deal with a model with an s -channel. This allows us to study a model with real intermediate states in the CTP formalism. Additionally, we deal with a situation, where the dark matter and not only particles from the thermal bath appear in the loop of the DM self energy. This requires us to rederive the kinetic equation governing freeze-in production in a more general setting.

The freeze-in of SSDM is a rather simple and well studied model. In depth-precision calculations have for example been performed in [10]. We improve upon the previous work, by performing the calculations from the CTP formalism instead of treating thermal effects through the inclusion of thermal masses. Using resummed propagators also treats the RIS problem and we do not have to rely on a specific RIS subtraction scheme. As in [10], we treat the electro-weak phase transition by calculating a temperature dependent effective Higgs potential. However, we will take greater care in the choice of perturbation scales and also treat effects from the Higgs self-coupling, which are relevant for currently observed Higgs masses.

The rest of this thesis is structured as follows: Chapter 2 discusses the DM freeze-in calculations in the standard Boltzmann equation formalism. Sections 2.1 and 2.2 will give a brief

overview of our current knowledge of dark matter and also introduce the freeze-in mechanism. Section 2.3 introduces the scalar singlet model in which all further calculations are performed. We introduce the semi-classical Boltzmann equation in section 2.4 and explicitly perform the necessary calculations in the following. In section 2.8 we highlight the problems caused by real intermediate states and introduce some common solutions.

While Chapter 2 is focused on the standard analysis in the semi-classical formalism, we will turn towards methods from non-equilibrium or finite temperature field theory in chapter 3. Section 3.1 and section 3.2 will serve as an introduction to finite temperature field theory and the closed time path (CTP) formalism. Then an evolution equation for the dark matter density will be derived from the Kadanoff-Baym equation of the CTP formalism in section 3.3. Afterwards, we use the next part to calculate the relevant self energies and show in section 3.6, that terms known from the Boltzmann equation can be recovered in the CTP formalism, by performing an expansion of the occurring Higgs propagator. As another application of finite temperature field theory we also calculate the temperature dependent effective potential in section 3.7, whose development is relevant in a freeze-in scenario.

The numerical results of the above mentioned calculations are examined in chapter 4. Finally we will conclude in chapter 5 with an overview of our results and use chapter 5 to point out some interesting ways to continue the present work.

2 Dark Matter freeze-in in the Boltzmann equation formalism

2.1 Dark Matter

2.1.1 Indications of the existence of Dark Matter

In the 21st century, dark matter is a stable constituent of our standard cosmological model [5]. Dark matter hereby refers to any kind of matter which has a gravitational effect on our visible universe but has no (or very weak) other interactions. Until today, there has been neither a direct nor an indirect detection of dark matter and it remains a mystery what dark matter actually is. However, there are multiple strong arguments to assume the existence of dark matter. A comprehensive history of our understanding of dark matter can be found in [25] and [5] which are used as an orientation in the following. Herein, we will only give an overview over the most significant experimental indications of dark matter.

One of the first concrete indications for the existence of dark matter was the rotational velocity of the Milky Way observed in the 1930s [26]. The mass required to explain the velocities in the outer parts of the galaxy was significantly larger than the one inferred from observations of luminous stars. The method has been further refined in the past decades both in the Milky Way [27] as well as beyond [28], confirming the observations of flat rotational curves at high distances to the center. However, the flattened rotational curves are challenged for far away galaxies, leading to the conclusion that dark matter density might vary throughout the universe [29].

Another early indication of dark matter, which also showed a significantly larger abundance than visible matter was discovered by Zwicky in the 1930s [30] [31]. Zwicky applied the virial theorem of thermodynamics to the Coma cluster. From its relative velocity distribution he received a very large mass to luminosity estimation in the cluster. While he grossly overestimated the amount of matter in the Coma cluster, due to the use of contemporary values of the Hubble parameter, modern analyses using the virial theorem still agree with the necessity of significant amounts of dark matter [32].

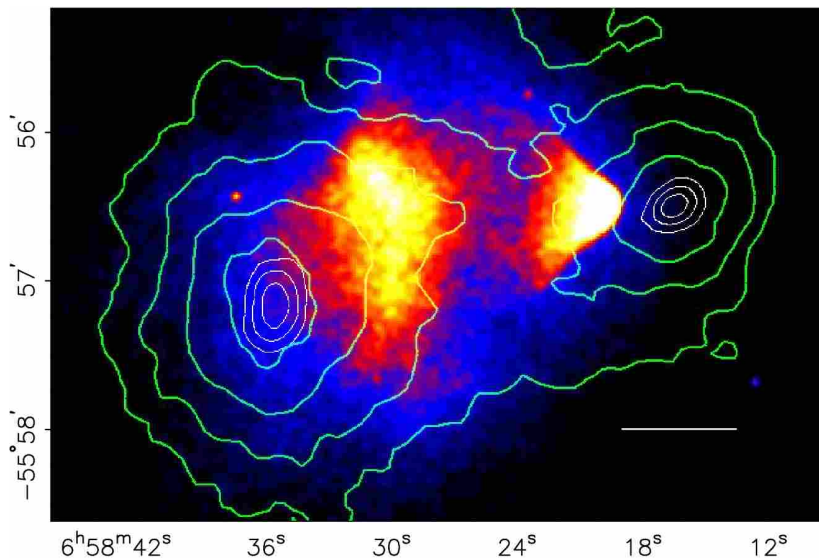


Figure 2.1: Gravitational lensing analysis of the Bullet Cluster. The underlying image is from the Chandra X-Ray Observatory and the green contours show different values of the magnification due to the lensing. Image taken from [34].

Perhaps one of the strongest indications of the existence of dark matter is given by our observations of gravitational lensing. Hereby, light is deflected or bend through the gravitational effects predicted by Einsteins theory of relativity. While initial attempts to find dark matter through gravitational micro lensing of individual large objects were unsuccessful [33], more recent observations of the bullet cluster show convincing evidence for the existence of dark matter [34]. This unique cluster is formed from the collision of two former clusters, leading to the spatial separation of luminous and dark matter components, which can be observed through their gravitational lensing effect as seen in figure 2.1.

Another strong indication forbidden the existence of dark matter can be obtained from the analysis of the cosmic microwave background (CMB). The temperature anisotropies of the CMB can be related to density fluctuations in the early universe. An analysis of the multipole expansion yields values for dark energy, as well as baryonic and non-baryonic matter densities of the universe in the Λ CDM model. This also yields the currently most accurate value for the dark matter relic density in our universe given by $\Omega_{CDM}h^2 = 0.1198 \pm 0.0012$ [3]. Here, $h \approx 0.67$ is the reduced Hubble constant.

For the sake of completeness, it should be mentioned that some of the above observations can also be explained through theories of modified gravity (MOND) [35]. MOND theories yield particulary good predictions for the dynamics and rotational curves of galaxies. However, none of the current MOND theories can explain the dynamics of galaxy clusters without also

including dark matter [36]. As such, the existence of dark matter is very well motivated and impacts of modified gravity shall be ignored in the rest of this thesis.

2.1.2 Dark matter candidates

All of the above tells us that an extra mass component which we call dark matter should exist in our universe. However, it does not tell us what dark matter actually is. Due to the lack of any direct or indirect detection to date, the exact properties of dark matter remain unknown, yet there are a multitude of possible explanations. We shall mention some broad concepts here. For a very comprehensive review, see [5].

Dark matter candidates are most broadly classified by their mass and their resulting behavior. At high masses ($M_{Pl} \leq m \leq 10^{37}\text{kg}$), candidates are macroscopic objects which are either black holes or composite objects. The upper bound here stems from the fact that dark matter is necessary to explain the behavior of dwarf galaxies and should thus only account for part of their mass. At lower scales ($1\text{eV} \lesssim m < M_{Pl}$) dark matter candidates may be elementary particles. Here, the upper bound is motivated, since elementary particles with a mass $m > M_{Pl}$ would be black holes. At lower values of the mass ($10^{-21}\text{eV} < m \lesssim \text{eV}$) particles are considered to be fields. While the difference between particles and fields is not fundamental in QFT, the distinction is based merely on the typical interaction with atom scaled test objects. The lower bound of the overall possible dark matter spectrum is based again on dwarf galaxies. As dark matter has to exist in dwarf galaxies, its de Broglie wavelength has to fit inside the typical size of such a galaxy.

Of the first category, Massive Astrophysical Compact Halo Objects (MACHOs) i.e. ordinary cosmological objects (of baryonic origin), which barely interact with light, were extensively studied in the past [25]. However, today significant contributions to the dark matter abundance in the universe are ruled out both by observations from the CMB and calculations from Big Bang Nucleosynthesis (BBN), as well as from the (non-)observation of gravitational micro-lensing effects. However, if DM instead consists of matter that predates BBN, such as in the case of primordial black holes, it may still account for the DM in our universe. Dark matter could also consist of macroscopic objects formed out of DM particles. This setup has barely been studied, due to its complexity but is not excluded for our universe. [5]

A more recent field of research is brought on by field-like dark matter of which different axion models are the most popular. Such dark matter models are able to explain the cosmological

observations and might even be preferred by the observation of halos around dwarf galaxies [37] [38].

The most extensively studied regime of dark matter candidates falls to particle dark matter. This is generally realized in a model by adding one or more particles to the standard model (SM), which barely interact with the SM outside of gravity. This allows for a multitude of models which are in principle valid. For a long time, the most favored models belonged to the class of weakly interactive massive particles (WIMPs). WIMPs naturally generate the observed relic density in a freeze-out scenario. They arise, for example, in Supersymmetry and other SM extensions, which also target fine-tuning issues, such as the hierarchy problem [39] [40]. However, much of the expected parameter space for WIMPs has by now been excluded through direct detection experiments such as XENONnT [41]. Instead, in this thesis we will consider feebly interactive massive particles (FIMPs) as dark matter. Thus, the coupling between dark matter and the SM is even weaker (only feeble) and production is generally considered in a freeze-in setting. [42]

2.2 Freeze-in of FIMP dark matter

As mentioned in the previous section, the most commonly studied dark matter production mechanism is the freeze-out production [7] [8] [9]. Here, dark matter is assumed to be abundant and in thermal equilibrium with the SM at high temperature. Following its distribution function, the dark matter abundance will fall with falling temperature until the coupling strength between DM and SM falls below the Hubble expansion $\langle n_{DM}\sigma \rangle \lesssim H$, effectively decoupling the DM from the rest of the particle species [5]. This leaves a “frozen-out” DM density behind which can be observed as the current DM relic density after further dilution due to the expansion of the universe.

Freeze-out scenarios in which WIMPs are the natural candidates for dark matter have been the dominantly studied scenarios for years. By now however, as discussed in section 2.1.2, large parts of the parameter space for WIMPs have been ruled out by experiments. This naturally shifts the focus towards different models and production mechanisms.

One of these different production mechanisms which has gained popularity in recent years is the freeze-in of dark matter [43]. Here, it is assumed, that the dark matter particle has only a very small (feeble) coupling to the standard model. For this reason, dark matter candidates in freeze-in scenarios are generally referred to as feebly interactive massive particles (FIMPs). Furthermore, the dark matter is assumed to have only a vanishing density at some early time

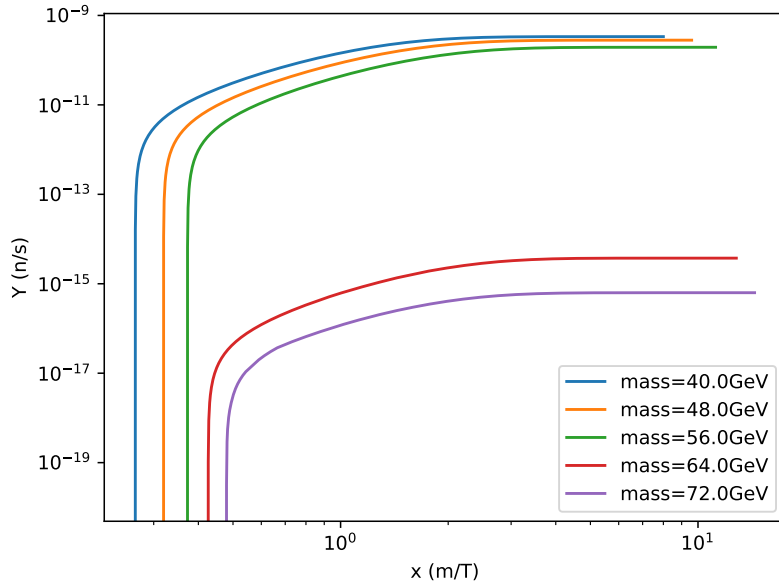


Figure 2.2: Typical evolution of the DM density in a freeze-in scenario. Here plotted is Y (density divided by the entropy density of the universe) against x (dark matter mass divided by Temperature) for different dark matter masses. The reached densities are significantly lower for high dark matter masses, since resonant processes are forbidden in these scenarios.

of the universe which is typically taken shortly after reheating. Although the coupling to the SM is small, it allows for some DM production as the universe cools down (the dark matter freezes in). It should be noted that, due to the feeble coupling to the SM, the DM particle never reaches the thermal equilibrium of the SM.

Typical evolutions of the dark matter density in a freeze-in scenario are shown in figure 2.2. As we can see, the production of the dark matter takes place predominantly at high temperatures ($T > m_{DM}$). This is a major difference to freeze-out processes, where typically lower temperature processes dominate and requires the treatment of high temperature effects.

Freeze-in scenarios can generally be realised in the same kind of models as freeze-out scenarios, as long as the couplings of the DM to the SM can be reasonably assumed to be small enough. As such, freeze-in scenarios have been studied in a whole host of different models. In many cases, one relies on mediators to motivate the small couplings [44, 45]. But scenarios without mediators are also studied [46, 47, 48]. In this thesis we will consider the freeze-in of dark matter described in the scalar singlet model which is introduced in the next section.

2.3 Scalar singlet dark matter model

As in [10, 49, 50], we will consider the scalar singlet dark matter (SSDM) model for our calculations. The SSDM is a rather simple model of dark matter which provides a minimal extension of the standard model [51]. Due to its simplicity, the SSDM is a widely studied model. By now, the SSDM is very strongly constrained in a freeze-out scenario [52]. However, the freeze-in scenario we are considering in this thesis is significantly less constrained. This is mostly due to the many orders smaller coupling between the dark matter and the SM. Such a freeze-in of scalar singlet dark matter has first been analysed in [24], but has since been investigated in a number of works.

Here, we will give a brief overview over the studied model. In the SSDM model, one additional scalar singlet S , which is stabilised by a \mathbb{Z}_2 symmetry and thus only couples to the standard model Higgs boson, is added to the SM. This is our dark matter candidate. The most general Lagrangian before electroweak symmetry breaking (EWSB) [10, 53] reads

$$\mathcal{L} = \mathcal{L}_{SM} + \frac{1}{2}\partial_\mu S \partial^\mu S - \frac{1}{2}\mu_S^2 S^2 - \frac{1}{2}\lambda_{hS} S^2 |H|^2 - \frac{1}{4}\lambda_S S^4. \quad (2.1)$$

Before EWSB, there is only a quartic coupling between 2 Higgs and 2 DM particles. After EWSB, we may write in unitary gauge $\sqrt{2}H^\dagger \rightarrow (h, 0)$. This allows us, to write the Lagrangian as:

$$\mathcal{L} = \mathcal{L}_{SM} + \frac{1}{2}\partial_\mu S \partial^\mu S - \frac{1}{2}\mu_S^2 S^2 - \frac{1}{4}\lambda_{hS} S^2 h^2 - \frac{1}{4}\lambda_S S^4. \quad (2.2)$$

The total scalar potential may be written as

$$V = \frac{1}{2}\mu_S^2 S^2 + \frac{1}{4}\lambda_{hS} S^2 h^2 + \frac{1}{4}\lambda_S S^4 + \frac{1}{4}\lambda_h (h^2 - v^2(T))^2. \quad (2.3)$$

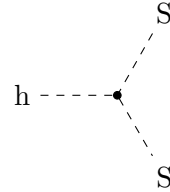
The last term is part of the SM higgs potential. Here, h is still a field centered around 0. It is more common (and useful) to shift the Higgs field by its vacuum expectation value (VEV) $h \rightarrow h + v(T)$. The potential then turns into

$$V = \frac{1}{2}\left(\mu_S^2 + \frac{1}{2}\lambda_{hS}v^2(T)\right)S^2 + \frac{1}{2}\lambda_{hS}v(T)S^2h + \frac{1}{4}\lambda_{hS}S^2h^2 + \frac{1}{4}\lambda_S S^4 + V_h, \quad (2.4)$$

where $V_h = \frac{\lambda v(T)^2}{2}h^2 + \frac{\lambda v(T)}{2}h^3 + \frac{\lambda}{8}h^4$ is the standard model Higgs potential. In the equation above, we can identify

$$m_s(T) = \sqrt{\mu_S^2 + \frac{1}{2}\lambda_{hS}v^2(T)} \quad (2.5)$$

as the temperature dependent mass of the dark matter scalar. The self-coupling terms of the Higgs and DM are irrelevant for our considerations. The above yields the following two new relevant couplings:



$$= i\lambda_{hS}v(T) \quad (2.6)$$



$$= i\lambda_{hS} \quad (2.7)$$

Of course, the coupling to the Higgs further allows an interaction with all other standard model particles. Most importantly, DM production of the kind $X, \bar{X} \rightarrow S, S$ is allowed for any massive SM particle X . However, it should be stated again that these couplings only exist at temperatures below EWSB. In principle, one should divide freeze-in calculations of SSDM into a regime above EWSB, where only the $S^2|H|^2$ vertex exists, and the calculations below EWSB. However, as seen in [10], the DM generation at temperatures above EWSB only matter for high DM masses $m_S \approx 300$ GeV. These will not be considered in this thesis where the focus will be near the resonant regime. Instead, we assume that no dark matter was produced before EWSB and we will just consider the production after EWSB.

2.4 Relic density calculations in the Boltzmann equation formalism

The most common procedure to calculate dark matter and other particle densities is the Boltzmann equation formalism, which will be explained in the following. The discussion will follow closely the ones given in [8] and [54]. In its most general form, the Boltzmann equation, which is an evolution equation for the distribution function, can be written as

$$\mathbf{L}[f] = \mathbf{C}[f]. \quad (2.8)$$

Here $\mathbf{C}[f]$ is the collision operator, which describes changes due to the scattering of different particles. $\mathbf{L}[f]$ on the other hand is the Liouvillian, which describes the total time evolution of the phase space distribution function f , $\mathbf{L}[f] = \frac{df}{dt}$. The first thing to consider is that the expansion of the universe has a relevant impact on the dark matter density in our universe.

A simple and typically used description of the expansion of the universe is the Friedmann-Lemâitre-Robertson-Walker (FLRW) metric [55]. For zero curvature K , we can write the FLRW metric as

$$ds^2 = dt^2 - a(t)^2 d|\vec{x}|^2. \quad (2.9)$$

To understand the impact of the background metric on the Boltzmann equation, we should consider a GR formulation, as it is done in [54]. However, to receive a covariant expression, we cannot simply write $\frac{df}{dt}$. We should instead write the derivation with respect to some affine parameter λ . We then have

$$\frac{df}{d\lambda} = \frac{dx^\mu}{d\lambda} \frac{\partial f}{\partial x^\mu} + \frac{dp^\mu}{d\lambda} \frac{\partial f}{\partial p^\mu}. \quad (2.10)$$

We may choose our normalisation of λ such that

$$\frac{dx^\mu}{d\lambda} = p^\mu \quad (2.11)$$

and

$$\frac{dp^\mu}{d\lambda} + \Gamma_{\alpha\beta}^\mu p^\alpha p^\beta = 0 \quad (2.12)$$

which leads to

$$\frac{df}{d\lambda} = p^\mu \frac{\partial f}{\partial x^\mu} - \Gamma_{\alpha\beta}^\mu p^\alpha p^\beta \frac{\partial f}{\partial p^\mu}. \quad (2.13)$$

Since we assume isotropic density functions, it is $f = f(t, E)$ and we have

$$\frac{df}{d\lambda} = p^0 \frac{\partial f}{\partial t} - \Gamma_{\alpha\beta}^0 p^\alpha p^\beta \frac{\partial f}{\partial p^0} = p^0 \frac{\partial f}{\partial t} - \dot{a} a |\vec{p}|^2 \frac{\partial f}{\partial p^0}. \quad (2.14)$$

Where the Christoffel symbols for a FLRW metric with $K = 0$ [8] [54]

$$\Gamma_{0\mu}^0 = 0, \quad \Gamma_{ij}^0 = -\frac{\dot{a}}{a} g_{ij} = \dot{a} a \delta_{ij} \quad (2.15)$$

have been used.

We may additionally use that the energy appearing above is already the physical energy, while the momentum corresponds to the physical (proper) momentum as $|\vec{p}| = \frac{1}{a} |\vec{p}|_{ph}$. We receive

$$\frac{df}{d\lambda} = p^0 \frac{\partial f}{\partial t} - H |\vec{p}|_{ph}^2 \frac{\partial f}{\partial E} \quad (2.16)$$

with the Hubble constant $H = \frac{\dot{a}}{a}$. We will drop the ph notation for the physical momentum in the following.

Integrating this expression and using the definition of the number density

$$n(t) = \frac{g}{(2\pi)^3} \int d^3p f(E, t) \quad (2.17)$$

we can write the left hand side of the Boltzmann equation as

$$\frac{g}{(2\pi)^3} \int \frac{d^3p}{E} \mathbf{L}[f] = \frac{g}{(2\pi)^3} \int \frac{d^3p}{E} \left(E \frac{\partial f}{\partial t} - H |\vec{p}|^2 \frac{\partial f}{\partial E} \right) \quad (2.18)$$

$$= \frac{\partial}{\partial t} n(t) - \frac{g}{(2\pi)^3} H \int d^3p \frac{|\vec{p}|^2}{E} \frac{\partial f}{\partial E}. \quad (2.19)$$

Here, the last integral can be transformed as

$$\int d^3p \frac{|\vec{p}|^2}{E} \frac{\partial f}{\partial E} = \int dE d\Omega |\vec{p}|^3 \frac{\partial f}{\partial E} \quad (2.20)$$

$$= \int d\Omega dE \underbrace{\left[\frac{\partial}{\partial E} (|\vec{p}|^3 f) - f \frac{\partial}{\partial E} (E^2 - m^2)^{3/2} \right]}_{=0} \quad (2.21)$$

$$= - \int d\Omega dE f 3E |\vec{p}| = -3 \int d^3p f. \quad (2.22)$$

This allows us to write the Boltzmann equation as

$$\frac{\partial n}{\partial t} - 3Hn = \frac{g}{(2\pi)^3} \int \frac{d^3p}{E} \mathbf{L}[f] = \frac{g}{(2\pi)^3} \int \frac{d^3p}{E} \mathbf{C}[f] := \gamma_{DM}, \quad (2.23)$$

where we defined the right hand side as γ_{DM} . Often, one instead formulates the Boltzmann equation in terms of $Y = \frac{n}{s}$ (e.g. [6], [50]), where s is the comoving entropy density of the universe, which adheres to the property $sR^3 = \text{const}$. This allows to write the left hand side of equation (2.23) as $s\dot{Y}$, since

$$s\dot{Y} = s \frac{\partial}{\partial t} \left(\frac{n}{s} \right) = \dot{n} \frac{s}{s} + sn \frac{\partial}{\partial t} \frac{1}{s} \quad (2.24)$$

$$= \dot{n} + sn \frac{\partial}{\partial t} \frac{R^3}{sR^3} = \dot{n} + sn \frac{1}{sR^3} \frac{\partial R^3}{\partial t} = \dot{n} + 3Hn. \quad (2.25)$$

Furthermore, we want to express the Boltzmann equation in terms of $x = \frac{m}{T}$ instead of time. Here m could in principle be any mass scale, but we will here choose it as the mass of the dark matter candidate. In cases where the DM mass depends on the temperature, we will choose $m = m_{DM}(T = 0)$, as it is only important to fix one constant scale. Using again the

conservation of entropy

$$0 = \frac{d}{dx}(sR^3) = R^3 \frac{ds}{dx} + 3sR^2 \frac{dR}{dx} \quad (2.26)$$

$$\iff \frac{dR}{dx} = -\frac{ds}{dx} \frac{R}{3s}, \quad (2.27)$$

we can write the derivative on the left hand side of the Boltzmann equation as

$$\frac{dY}{dt} = \frac{dY}{dx} \frac{dx}{dR} \frac{dR}{dt} = \frac{dY}{dx} \frac{1}{\frac{ds}{dx} \frac{R}{3s}} H R = -\frac{dY}{dx} \frac{3Hs}{\frac{ds}{dx}}. \quad (2.28)$$

This allows us to write the entire Boltzmann equation as

$$\frac{dY}{dx} = -\frac{ds}{dx} \frac{1}{3s^2 H} \gamma_{DM}. \quad (2.29)$$

As in [56], we can describe the Hubble expansion rate appearing in equation (2.29) as $H = \sqrt{\rho/(M_{Pl})}$, where ρ is the energy density. The energy density and the entropy density can be described through the SM effective degrees of freedom $h_{eff}(T)$ and $g_{eff}(T)$ as

$$\rho = g_{eff}(T) \frac{\pi^2}{30} T^4 \quad (2.30)$$

$$s = h_{eff}(T) \frac{2\pi^2}{45} T^3. \quad (2.31)$$

The degrees of freedom are taken from the lattice calculations tabulated in [57]. Using the form of the entropy density given above, we have $\frac{ds}{dx} = -s \frac{T}{m} \left(3 + \frac{d \ln(h_{eff})}{dT} T \right)$ and the Boltzmann equation turns into

$$\frac{dY}{dx} = \frac{1}{Hsx} \left(1 + \frac{1}{3} \frac{d \ln(h_{eff})}{dT} \frac{m}{x} \right) \gamma_{DM}. \quad (2.32)$$

If we solve this equation for Y , we may calculate the relic density by writing [6]

$$\Omega = \frac{\rho_0}{\rho_c} = \frac{mn_0}{\rho_c} = \frac{mY_0 s_0}{\rho_c}. \quad (2.33)$$

In practice, we will for practical reasons not solve equation (2.32) up until current temperatures T_0 . Instead, the density is evaluated down to low temperatures $T_1 \approx 5 \text{ GeV}$, where DM production is negligible. The produced density is then evolved solely through the expansion of the universe as in [56]. We can finally write the relic density as

$$\Omega h^2 = \frac{m_{DM} Y_{DM}(T_1) s_0}{\rho_c / h^2} \frac{h_{eff}(T_0)}{h_{eff}(T_1)} \left(\frac{T_0}{T_1} \right)^3. \quad (2.34)$$

2.5 Scattering terms in the Boltzmann equation

For now we only looked at the left hand side of the Boltzmann equation. However, to evaluate any results, we have to understand the scattering term $\gamma_{DM} = \frac{g}{(2\pi)^3} \int \frac{d^3p}{E} \mathbf{C}[f]$ on the right hand side of equation (2.23). The standard analysis is due to Gelmini and Gondolo [6], but we will repeat the calculations here. This will allow us to understand where differences occur when quantum statistics are considered instead of the Maxwell-Boltzmann limit.

γ_{DM} can be written as a sum over all processes, in which the particle is created, annihilated or elastically scattered, although the latter is not relevant for the overall particle density, only for the momentum distribution of the particle species. For general processes of particles i scattering to particles j , we can write the scattering term as [8]

$$\gamma_{DM} = \sum_{\text{all processes}} \int \prod_{i,j} d\Pi_i d\Pi_j (2\pi)^4 \delta^{(4)}(\sum_i p_i - \sum_j p_j) \quad (2.35)$$

$$[|M|_{i \rightarrow j}^2 \prod_i f_i \prod_j (1 \pm f_j) - |M|_{j \rightarrow i}^2 \prod_j f_j \prod_i (1 \pm f_i)] \quad (2.36)$$

$$= \sum_{\text{all processes}} \int \prod_{i,j} d\Pi_i d\Pi_j (2\pi)^4 \delta^{(4)}(\sum_i p_i - \sum_j p_j) \quad (2.37)$$

$$|M|^2 [\prod_i f_i - \prod_j f_j], \quad (2.38)$$

where the last step holds under the assumption of T or CP invariance, such that

$|M|_{i \rightarrow j}^2 = |M|_{j \rightarrow i}^2 := |M|^2$. Here and in the rest of the thesis, it is understood, that $d\Pi_p = \frac{1}{(2\pi)^3} \frac{d^3p}{2E}$ is the integration over the phasespace volume. Additionally, $|M|^2$ here describes the summed not averaged matrix element as in [56]. Furthermore, we ignored the Pauli blocking and Bose enhancement factors for all particles, allowing us to set $1 \pm f_k \approx 1$. For small occupations, far from Bose condensation or Fermi degeneracy, this is a good and common approximation [8]. It should be noted that the sum over all relevant processes includes a given process as often as the investigated particle species appears in the process. I.e., if we are interested in the evolution of the dark matter density and a certain process involves n DM particles, it has to be counted n times.

First, we take a look at a $1 \rightarrow 2$ (as for example $h \rightarrow S, S$) decay, where both outgoing particles are assumed to be of the same mass (as for a particle-antiparticle pair). In our case, the outgoing particles are dark matter candidates with a low phase space density. As such, we will ignore possible backscattering events. If we assume Boltzmann statistics, the

scattering term reduces to

$$\gamma_{DM} = \int d\Pi_1 d\Pi_2 d\Pi_0 (2\pi)^4 \delta^{(4)}(p_1 + p_2 - p_0) |M|^2 f_0 \quad (2.39)$$

$$= \int d\Pi_0 f_0 2m_0 \Gamma_{0 \rightarrow 1,2} \quad (2.40)$$

$$= \int \frac{d|\vec{p}|}{(2\pi)^3} \frac{d\Omega}{2E_0} \Gamma_{0 \rightarrow 1,2} f_0 2m_0 |\vec{p}|^2 \quad (2.41)$$

$$= \int \frac{dE}{2\pi^2} |\vec{p}| \Gamma_{0 \rightarrow 1,2} f_0 m_0 \quad (2.42)$$

$$= \frac{m_0 \Gamma}{2\pi^2} \int dE (E^2 - m_0^2)^{1/2} e^{-E/T} = \left| x = \frac{E}{m_0}, dx = \frac{1}{m_0} dE \right| \quad (2.43)$$

$$= \frac{m_0^3 \Gamma}{2\pi^2} \int_1^\infty dx (x^2 - 1)^{1/2} e^{-xm_0/T} \quad (2.44)$$

$$= \frac{m_0^2 \Gamma}{2\pi^2} TK_1\left(\frac{m_0}{T}\right) \quad (2.45)$$

Here $\Gamma_{0 \rightarrow 1,2}$ is the decay width of the original particle 0 to the two new particles 1, 2. We used the definition of the modified Bessel function of the second kind and first degree

$$K_1(z) = \frac{\sqrt{\pi}}{\frac{1}{2}!} \left(\frac{1}{2}z\right) \int_1^\infty e^{-xz} (x^2 - 1)^{1/2} dx. \quad (2.46)$$

If we do not assume Boltzmann-Statistics, the integral cannot be solved analytically. Instead, we can see from equation (2.42), that we have to solve numerically the integral

$$\gamma_{DM} = \frac{m_0 \Gamma}{2\pi^2} \int dE \sqrt{E^2 - m_0^2} f_B(E). \quad (2.47)$$

We will look at the determination of the specific decay rates later and will first investigate the calculations necessary to account for $2 \rightarrow 2$ processes. There are multiple relevant $2 \rightarrow 2$ processes in our case, which generally take the form $X, \bar{X} \rightarrow S, S$ for some SM particle X and the darkmatter S . Apart from the Higgs annihilation, there are only s-channel processes, with a Higgs as the intermediary particle. With the same assumptions as above, we can write for the $2 \rightarrow 2$ processes

$$\gamma_{DM} = \int d\Pi_1 d\Pi_2 d\Pi_3 d\Pi_4 (2\pi)^4 \delta^{(4)}(p_1 + p_2 - p_3 - p_4) |M|^2 f_1 f_2 \quad (2.48)$$

$$= \int d\Pi_1 d\Pi_2 4\mathcal{F} \sigma_{1,2 \rightarrow 3,4} f_1 f_2. \quad (2.49)$$

Here, $\sigma_{1,2 \rightarrow 3,4}$ is the cross section of the scattering process and we will suppress its indices in the following. Additionally, $\mathcal{F} = \sqrt{(p_1 \cdot p_2)^2 - m_1^2 m_2^2}$ is the Lorentz invariant flux, which is sometimes written as $\mathcal{F} = E_1 E_2 v_{\text{Mol}}$. For this reason, the production density is often written

as

$$\gamma_{DM} = \int \frac{d^3p_1}{(2\pi)^3} \frac{d^3p_2}{(2\pi)^3} v_{M\phi} \sigma_{1,2 \rightarrow 3,4} f_1 f_2. \quad (2.50)$$

The formulation in equation (2.50) has reached widespread popularity through a similar use in [6]. However, we will avoid it in the following, as it divides the Lorentz-invariant \mathcal{F} into two non Lorentz-invariant parts. This unnecessarily adds to the confusion which might be created by the Lorentz (in-)dependence of the occurring cross section σ .¹ Additionally $v_{M\phi}$ is often described as the relative velocity. This is a dangerous statement, as it is not true in a general frame. Some authors argue, that the use of $v_{M\phi}$ should be avoided in its entirety [60].

For these reasons, we will avoid the formulation of $v_{M\phi}$ and instead continue our calculation from equation (2.49). We can rewrite the integral measure as

$$d^3p_1 d^3p_2 = d|\vec{p}_1| d|\vec{p}_2| d\Omega_1 d\Omega_2 |\vec{p}_1|^2 |\vec{p}_2|^2 \quad (2.51)$$

$$= d|\vec{p}_1| d|\vec{p}_2| d\phi_1 ds d\Omega_2 \frac{1}{2} |\vec{p}_1| |\vec{p}_2| \quad (2.52)$$

$$= 4\pi^2 d|\vec{p}_1| d|\vec{p}_2| ds |\vec{p}_1| |\vec{p}_2| \quad (2.53)$$

$$= 4\pi^2 dE_1 dE_2 ds E_1 E_2 \quad (2.54)$$

$$= 2\pi^2 dE_+ dE_- ds E_1 E_2, \quad (2.55)$$

where we used the non-trivial substitutions

$$s = (p_1 + p_2)^2 = p_1^2 + p_2^2 + 2E_1 E_2 - 2|\vec{p}_1| |\vec{p}_2| \cos \theta \quad (2.56)$$

$$\Rightarrow ds = 2|\vec{p}_1| |\vec{p}_2| \sin \theta d\theta \quad (2.57)$$

and

$$E_{\pm} = E_1 \pm E_2 \quad (2.58)$$

$$\Rightarrow dE_+ dE_- = 2dE_1 dE_2. \quad (2.59)$$

¹Peskin&Schröder [58] derive a Lorentz dependent result of the crosssection and argue that this is expected, as it is also the behavior of a classical crosssection. However, Weinberg [59] demands crosssections to be Lorentz invariant and defines the Flux accordingly. The definition by Weinberg is also generally taken in the dark matter community [6] [5]. While the results for the crosssection cited here are equivalent in the context of collider physics, where all events happen along one axis, they are not in the context of dark matter generation, where processes might take place at arbitrary angles. However, under proper definition of the flux \mathcal{F} this does not have an impact on equation (2.49).

If we rewrite the Flux for equal masses m_1, m_2 , using

$$(p_1 \cdot p_2)^2 = \frac{1}{4}(s^2 + m_1^2 + m_2^2) - \frac{1}{2}(sm_1^2 + sm_2^2 + m_1^2 m_2^2) \quad (2.60)$$

$$= \frac{s^2}{4} - m^2 s + m^2 \quad (2.61)$$

$$\Rightarrow \mathcal{F} = \sqrt{\frac{s^2}{4} - sm^2} \quad (2.62)$$

and assume that the initial particles are in equilibrium and obey Boltzmann statistics, so $f_1 f_2 = e^{-\frac{E_{\pm}}{T}}$, we can rewrite the scattering term for an s-channel process as

$$\gamma_{DM} = \int \frac{d^3 p_1}{(2\pi)^3} \frac{d^3 p_2}{(2\pi)^3} \frac{4\mathcal{F}}{2E_1 2E_2} \sigma_{1,2 \rightarrow 3,4} f_1 f_2 \quad (2.63)$$

$$= \frac{2\pi^2}{(2\pi)^6} \int_{\sqrt{s}}^{\infty} dE_+ \int_{-k}^k dE_- \int_{4m^2}^{\infty} ds \sigma \sqrt{\frac{s^2}{4} - sm^2} e^{-\frac{E_{\pm}}{T}} \quad (2.64)$$

$$= \frac{1}{(2\pi)^4} \int_{\sqrt{s}}^{\infty} dE_+ \int_{4m^2}^{\infty} ds \sigma \sqrt{\frac{s^2}{4} - sm^2} e^{-\frac{E_{\pm}}{T}} \sqrt{1 - \frac{4m^2}{s}} \sqrt{E_+^2 - s} \quad (2.65)$$

$$= \frac{1}{(2\pi)^4} \int_{4m^2}^{\infty} ds \sigma \frac{\sqrt{s}}{2} (s - 4m^2) \int_1^{\infty} dx \sqrt{s(x^2 - 1)} e^{-\frac{x\sqrt{s}}{T}} \quad (2.66)$$

$$= \frac{1}{(2\pi)^4} \int_{4m^2}^{\infty} ds \sigma \frac{s}{2} (s - 4m^2) \int_1^{\infty} dx \sqrt{x^2 - 1} e^{-\frac{x\sqrt{s}}{T}} \quad (2.67)$$

$$= \frac{1}{(2\pi)^4} \int_{4m^2}^{\infty} ds \sigma (s - 4m^2) \frac{\sqrt{s}}{2} TK_1\left(\frac{\sqrt{s}}{T}\right) \quad (2.68)$$

$$= \frac{1}{(2\pi)^4} \int_{4m^2}^{\infty} ds \sigma \mathcal{F} \sqrt{s - 4m^2} TK_1\left(\frac{\sqrt{s}}{T}\right). \quad (2.69)$$

Here, the boundaries for the E_+ and s integral are clear. The boundaries for the E_- integral, with $k = \sqrt{1 - \frac{4m^2}{s}} \sqrt{E_+^2 - s}$ can be figured out, by considering that $|E_-|$ is maximal, if one of the initial particles is at rest e.g. $p_1 = (m_f, 0)$, while the other has some momentum $p_2 = (E_2, \vec{p}_2)$. Then, it is

$$|E_-| = |E_1 - E_2| = \sqrt{m_f^2 + |\vec{p}_2|^2} - m_f \quad (2.70)$$

$$E_+ = m_f + \sqrt{m_f^2 + |\vec{p}_2|^2} \quad (2.71)$$

$$s = (p_1 + p_2)^2 = E_+^2 - |\vec{p}_2|^2 = (m_f + \sqrt{m_f^2 + |\vec{p}_2|^2})^2 - |\vec{p}_2|^2 = 2m_f E_+ \quad (2.72)$$

and it is in the maximal case

$$|E_-| = \sqrt{|E_-|} \sqrt{\frac{|\vec{p}_2|^2 |E_-|}{m_f^2 + |\vec{p}_2|^2 - m_f^2}} = \sqrt{|E_-|} \sqrt{\frac{|\vec{p}_2|^2 |E_-|}{E_+ |E_-|}} \quad (2.73)$$

$$= \sqrt{2mf|E_-|} \sqrt{\frac{|\vec{p}_2|^2}{2mfE_+}} = \sqrt{s - 4m_f^2} \sqrt{\frac{|\vec{p}_2|^2}{s}} \quad (2.74)$$

$$= \sqrt{1 - \frac{4m^2}{s}} \sqrt{E_+^2 - s}. \quad (2.75)$$

In the case, where we do not assume Boltzmann statistics, we need to identify the occurring ingoing particles. In our case, only the case of two ingoing fermions of identical mass is relevant. In this case, it is

$$\gamma_{DM} = \int \frac{d^3 p_1}{(2\pi)^3} \frac{d^3 p_2}{(2\pi)^3} \frac{4\mathcal{F}}{2E_1 2E_2} \sigma f_1 f_2 \quad (2.76)$$

$$= \frac{4\pi^2}{(2\pi)^6} \int_{m_1}^{\infty} dE_1 \int_{\max(\sqrt{s-E_1}, m_2)}^{\infty} dE_2 \int_{4m^2}^{\infty} ds \sigma \mathcal{F} f_F(E_1) f_F(E_2) \quad (2.77)$$

$$= \frac{1}{(2\pi)^4} \int_{4m^2}^{\infty} ds \sigma \mathcal{F} F(s, m_1, m_2), \quad (2.78)$$

where $F(s, m_1, m_2)$ is the integral over the 2 Fermi distributions. We can use that

$$\int_A^{\infty} dE_2 f_F(E_2) = T \log\left(1 + e^{-A/T}\right), \quad (2.79)$$

such that:

$$F(s, m_1, m_2) = \int_{m_1}^{\infty} dE_1 \int_{\max(\sqrt{s-E_1}, m_2)}^{\infty} dE_2 f_F(E_1) f_F(E_2) \quad (2.80)$$

$$= \int_{m_1}^{\infty} dE_1 T \log\left(1 + e^{-\max(\sqrt{s-E_1}, m_2)/T}\right) f_F(E_1) \quad (2.81)$$

$$= \int_{\sqrt{s-m_2}}^{\infty} dE_1 f_F(E_1) T \log\left(1 + e^{-m_2/T}\right) \quad (2.82)$$

$$+ \int_{m_1}^{\sqrt{s-m_2}} dE_1 f_F(E_1) T \log\left(1 + e^{-(\sqrt{s-E_1})/T}\right) \quad (2.83)$$

$$= T^2 \log\left(1 + e^{-m_2/T}\right) \log\left(1 + e^{-(\sqrt{s-m_2})/T}\right) \quad (2.84)$$

$$+ \int_{m_1}^{\sqrt{s-m_2}} dE_1 f_F(E_1) T \log\left(1 + e^{-(\sqrt{s-E_1})/T}\right). \quad (2.85)$$

The second term in the above has to be solved numerically.

2.6 Relevant decay rates for Boltzmann-processes

As we had already seen in section 2.5, the scattering terms corresponding to $1 \rightarrow 2$ processes can be written in terms of decay rates. Furthermore, we will see in section 2.7 that it makes sense to write the s -channel crosssections occuring in the scattering terms for $2 \rightarrow 2$ processes in terms of decay rates of excited particles. We will use this section to calculate the relevant decay rates. In all of the relevant processes, the decaying particle is a Higgs and we can write the decay rate into two particles of identical mass m_X in terms of the squared matrix element as:

$$\Gamma = \int d\Gamma = \int |M|^2 \frac{1}{2m_h} \left(\frac{d^3p_1}{2E_1} \frac{d^3p_2}{2E_2} \frac{1}{(2\pi)^2} \delta^{(4)}(p_0 - p_1 - p_2) \right) \quad (2.86)$$

$$= \int |M|^2 \frac{1}{2m_h} \frac{1}{(2\pi)^2} \frac{d^3p_1}{2E_1} \frac{1}{2m_h} \delta(E_1 - \frac{m_h}{2}) \quad (2.87)$$

$$= |M|^2 \frac{1}{4m_h^2} \frac{1}{(2\pi)^2} 4\pi \int d|\vec{p}_1| \frac{|\vec{p}_1|^2}{2E_1} \delta(E_1 - \frac{m_h}{2}) \quad (2.88)$$

$$= |M|^2 \frac{1}{4m_h^2} \frac{1}{\pi} \int dE_1 \frac{\sqrt{E_1^2 - m_X^2}}{2} \delta(E_1 - \frac{m_h}{2}) \quad (2.89)$$

$$= |M|^2 \frac{1}{8m_h^2} \frac{1}{\pi} \sqrt{\frac{m_h^2}{4} - m_X^2} \quad (2.90)$$

$$= |M|^2 \frac{1}{m_h^2} \frac{1}{16\pi} \sqrt{m_h^2 - 4m_X^2}. \quad (2.91)$$

In the scalar singlet model, the only relevant $1 \rightarrow 2$ process for the production of dark matter is $h \rightarrow SS$. Here, the matrix element is simply

$$|M|^2 = \frac{1}{2} \lambda_{hs}^2 v(T)^2. \quad (2.92)$$

The factor $\frac{1}{2}$ occuring in the above is a symmetry factor appearing due to the 2 identical particles in the final state. However, it should be noted that the decay term also has to be counted twice in the Boltzmann equation, leading to an effective cancellation of the term. Following equation (2.91), we can write the decay rate as

$$\Gamma_{h \rightarrow SS} = \frac{\lambda_{hs}^2 v(T)^2}{m_h^2} \frac{1}{32\pi} \sqrt{m_h^2 - 4m_s^2}. \quad (2.93)$$

Further decay rates are only relevant in the context of the $2 \rightarrow 2$ cross sections and shall be discussed in the next section.

2.7 Relevant $2 \rightarrow 2$ cross sections

To evaluate the $2 \rightarrow 2$ scattering contributions to the freeze-in, we need to express the corresponding cross sections. The differential cross section for a $1, 2 \rightarrow 3, 4$ process is in general given as [61]

$$d\sigma = \frac{1}{4\mathcal{F}} |M|^2 d\Pi_{LIPS}, \quad (2.94)$$

where $|M|$ is the matrix element and \mathcal{F} is the flux as shown in section 2.5. Additionally, $d\Pi_{LIPS} = (2\pi)^4 \delta^4(\sum p) \prod_{\text{final states } j} \frac{d^3 p_j}{(2\pi)^j} \frac{1}{2E_j}$ is the Lorentz invariant phase space element. We can then write the total crosssection for DM production as

$$\sigma = \int d\sigma = \int \frac{1}{4\mathcal{F}} |M|^2 d\Pi_{LIPS} \quad (2.95)$$

$$= \int \frac{1}{4\mathcal{F}} |M|^2 (2\pi)^4 \delta^4(\sum p) \prod_{\text{final states } j} \frac{d^3 p_j}{(2\pi)^j} \frac{1}{2E_j} \quad (2.96)$$

$$= \int \frac{1}{4\mathcal{F}} |M|^2 \frac{1}{(2\pi)^2} \frac{d^3 p_3}{2E_3} d^4 p_4 \delta(p_4^2 - m_s^2) \delta^4(p_1 + p_2 - p_3 - p_4) \quad (2.97)$$

$$= \int \frac{1}{4\mathcal{F}} |M|^2 \frac{1}{(2\pi)^2} \frac{d^3 p_3}{2E_3} \delta((p_1 + p_2 - p_3)^2 - m_s^2). \quad (2.98)$$

We can evaluate the delta function in the CMS, by using

$$(p_1 + p_2 - p_3)^2 = (\sqrt{s} - E_3)^2 - |\vec{p}_3|^2 \quad (2.99)$$

$$= s + E_3^2 - 2\sqrt{s}E_3 - E_3^2 + m_s^2 \quad (2.100)$$

$$= s - 2\sqrt{s}E_3 + m_s^2 \quad (2.101)$$

which allows us to write

$$\delta((p_1 + p_2 - p_4)^2 - m_s^2) = \delta(s - 2E_3\sqrt{s}) = \frac{1}{2\sqrt{s}} \delta(E_3 - \frac{1}{2}\sqrt{s}). \quad (2.102)$$

With a spherical transformation of the integral and using that for incoming particles of equal mass $\mathcal{F} = \sqrt{\frac{1}{4}s^2 - sm_i^2}$, we can write the cross section as

$$\sigma = \int d\Omega dE_3 \frac{1}{4\mathcal{F}} |M|^2 \frac{1}{2(2\pi)^2} |\vec{p}_3| \frac{1}{2\sqrt{s}} \delta(E_3 - \frac{1}{2}\sqrt{s}) \quad (2.103)$$

$$= \int d\Omega \frac{1}{4\mathcal{F}} |M|^2 \frac{1}{16\pi^2} \sqrt{\frac{\frac{s}{4} - m_s^2}{s}} \quad (2.104)$$

$$= 4\pi |M|^2 \frac{1}{4\sqrt{\frac{1}{4}s^2 - sm_i^2}} \frac{1}{16\pi^2} \sqrt{\frac{\frac{s}{4} - m_s^2}{s}} \quad (2.105)$$

$$= |M|^2 \frac{1}{16\pi} \sqrt{\frac{s - 4m_s^2}{s - 4m_i^2}} \frac{1}{s}. \quad (2.106)$$

In total, the scattering term can also be expressed as

$$\gamma_{DM} = \frac{1}{512\pi^5} \int_{4m_{DM}^2}^{\infty} ds |M|^2 \frac{1}{\sqrt{s}} \sqrt{s - 4m_{DM}^2} \sqrt{s - 4m_f^2} T K_1\left(\frac{\sqrt{s}}{T}\right), \quad (2.107)$$

as for example in [43]. Alternatively, for a solely s -dependent matrix element and assuming T or CP symmetry, we may decompose the matrix-element. Then the cross section of the annihilation of standard model particles $x\bar{x}$ via the Higgs-channel can be factorised as [10]:

$$\sigma_{x\bar{x} \rightarrow ss} = \frac{1}{2} |M|^2 \frac{1}{16\pi} \sqrt{\frac{s - 4m_{DM}^2}{s - 4m_x^2}} \frac{1}{s} \quad (2.108)$$

$$= \frac{1}{2} \frac{|M_{ss \rightarrow h}|^2 |M_{h \rightarrow x\bar{x}^*}|^2}{(s - m_h^2)^2 + m_h^2 \Gamma_h^2} \frac{1}{16\pi} \sqrt{\frac{s - 4m_{DM}^2}{s - 4m_x^2}} \frac{1}{s} \quad (2.109)$$

$$= \frac{1}{2} \frac{|M_{ss \rightarrow h}|^2}{(s - m_h^2)^2 + m_h^2 \Gamma_h^2} \Gamma_{h \rightarrow x\bar{x}}^* \frac{1}{v_{M\phi l}} \frac{2}{\sqrt{s}} \sqrt{\frac{s - 4m_s^2}{s - 4m_x^2}} \quad (2.110)$$

$$\iff \sigma_{x\bar{x} \rightarrow ss} v_{M\phi l} = \frac{\lambda_{hs}^2 v^2}{\sqrt{s}} \frac{1}{(s - m_h^2)^2 + m_h^2 \Gamma_h^2} \Gamma_{h \rightarrow x\bar{x}}^* \sqrt{\frac{s - 4m_s^2}{s - 4m_x^2}} \quad (2.111)$$

Despite the discussion in section 2.5, we use the formulation with $v_{M\phi l} = \frac{2\sqrt{s - 4m_f^2}}{\sqrt{s}}$ here, as it is a quite common way to discuss cross sections in the context of Boltzmann equations. However, we can also write down the cross section without $v_{M\phi l}$ as

$$\sigma_{x\bar{x} \rightarrow ss} = \frac{1}{2} \frac{\lambda_{hs}^2 v^2}{(s - m_h^2)^2 + m_h^2 \Gamma_h^2} \Gamma_{h \rightarrow xx}^* \frac{\sqrt{s - 4m_s^2}}{s - 4m_f^2}. \quad (2.112)$$

The factor $\frac{1}{2}$ is due to the identical outgoing particles, but as above, the process also has to be counted twice for the evolution of the dark matter density. In the above Γ^* , always refers to a decay width, which is evaluated at the scale of the Mandelstam variable s instead

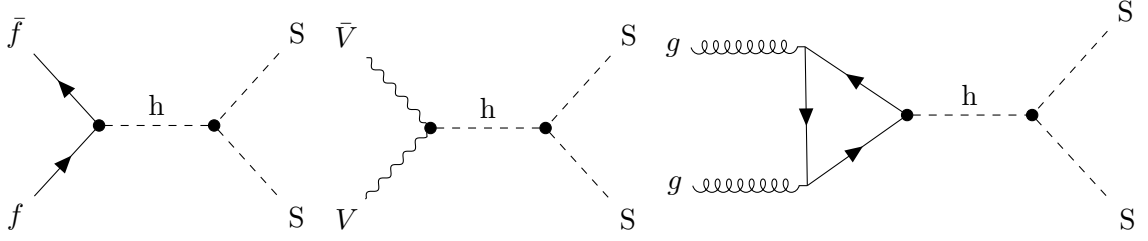


Figure 2.3: Relevant tree-level s-channel diagrams for DM creation. We have $2 \rightarrow 2$ production from the annihilation of fermions vector bosons and gluons. The gluon annihilation is technically not a tree-level process, but the quark-loop is treated as an effective tree-level coupling.

of the mass scale of the particle. It should be noted, that the above derivation relies on the circumstance, that the squared matrix element is purely s dependent. As we will see in the case of Higgs annihilation below, the integral of the cross section has to be solved explicitly for t- or u-channels.

The relevant s -channel processes are sketched in figure 2.3 and discussed in the following.

To describe the annihilation of two SM Fermions into dark matter $f\bar{f} \rightarrow SS$, we need to evaluate the decay rate $h \rightarrow f\bar{f}$. In this case, it is

$$iM_{h \rightarrow f\bar{f}} = -i \frac{\gamma_f}{\sqrt{2}} \bar{u}_f v_f \quad (2.113)$$

$$\Rightarrow |M_{h \rightarrow f\bar{f}}|^2 = \frac{\gamma_f^2}{2} N_c \text{Tr}[(\bar{u}v)^2], \quad (2.114)$$

where N_c is the number of colors of the fermion f and γ_f is the Yukawa coupling to the Higgs. With the cyclic property of the trace and the spinor identities, we have

$$\text{Tr}[(\bar{u}v)^2] = \text{Tr}[\bar{v}u\bar{u}v] = \text{Tr}[u\bar{u}v\bar{v}] \quad (2.115)$$

$$= \text{Tr}\left((\not{p}_1 + m)(\not{p}_2 - m)\right) \quad (2.116)$$

$$= \text{Tr}\left(\not{p}_1 \not{p}_2 - m^2 + \not{p}_1 m - \not{p}_2 m\right). \quad (2.117)$$

Using $\text{Tr}(\gamma^\mu) = 0$ and $\{\gamma^\mu, \gamma^\nu\} = 2g^{\mu\nu}\mathbb{1}$, as well as observing the process in the CMS system, where $p_0 = (m_h, 0, 0, 0)$ and $\vec{p}_1 = -\vec{p}_2$, as well as $E_1 = E_2 = m_h/2 := E$ we receive

$$\text{Tr}[(\bar{u}v)^2] = \text{Tr}(p_1 p_2 \mathbb{1} - m^2 \mathbb{1}) = 4(p_1 p_2 - m^2) \quad (2.118)$$

$$= 4(E^2 + |\vec{p}|^2 - m^2) = 4(2E^2 - 2m^2) = 4(s/2 - 2m^2) = 2(s - 4m^2). \quad (2.119)$$

In total, the squared matrix element then reads

$$|M_{h \rightarrow f\bar{f}}|^2 = \gamma_{\bar{f}}^2 N_c (s - 4m_f^2). \quad (2.120)$$

The decay width evaluated for $m = s$ is by equation (2.91)

$$\Gamma_{h \rightarrow f\bar{f}}^* = N_C \frac{\gamma_f^2}{16\pi} \frac{(s - 4mf^2)^{3/2}}{s}. \quad (2.121)$$

We follow the same procedure for the annihilation of vector bosons and gluons pictured in figure 2.3. For vector bosons V coupling to the Higgs, we have

$$M_{h \rightarrow V\bar{V}} = \epsilon_r^\mu \epsilon_s^\nu g^{\mu\nu} \frac{-iem_V}{\sin \theta_W}. \quad (2.122)$$

Since

$$\sum_{r,s} \epsilon_r^\mu \epsilon_s^\nu (\epsilon_r^\rho)^* (\epsilon_s^\eta)^* g^{\mu\nu} g^{\rho\eta} = (g^{\mu\rho} - \frac{p^\mu p^\rho}{m_V^2})(g^{\mu\rho} - \frac{p^\mu p^\rho}{m_V^2}) \quad (2.123)$$

$$= \frac{1}{4} \frac{s^2}{m_V^4} (1 - 4\frac{m_V^2}{s} + 12\frac{m_V^4}{s^2}), \quad (2.124)$$

as well as $\frac{e^2}{m_W^2 \sin^2 \theta_W} = \frac{4}{v^2}$, we can write

$$|M_{h \rightarrow VV}|^2 = \frac{\delta_V}{8} \frac{s^2 e^2}{m_V^2 \sin^2 \theta} (1 - 4\frac{m_V^2}{s} + 12\frac{m_V^4}{s^2}) \quad (2.125)$$

$$\Gamma_{h \rightarrow VV}^* = \frac{\sqrt{s}^3}{32\pi v^2} \delta_V \sqrt{1 - 4\frac{m_V^2}{s}} (1 - 4\frac{m_V^2}{s} + 12\frac{m_V^4}{s^2}), \quad (2.126)$$

with $\delta_Z = 1$, $\delta_W = 2$ due to the extra factor $\frac{1}{2}$ generated by the symmetry of the Z -boson decay.

Next, we derive the effective decay width of a Higgs decaying into two gluons, to describe the last diagram in figure 2.3. We can treat the coupling of 2 gluons to the Higgs via a quark triangle as an effective coupling, with the vertex factor $-4L_{GGH}(Q)\delta_{ab}(p_1 \cdot p_2 g^{\mu\nu} - p_1^\nu p_2^\mu)$. Here, $L_{GGH}(Q)$ is a scale dependent coupling parameter, which was taken from Micromegas [62]. The matrix element then takes the form

$$M_{h \rightarrow gg} = -\epsilon_{r,a}^\mu \epsilon_{s,b}^\nu 4L_{GGH} \delta_{ab} (p_1 \cdot p_2 g^{\mu\nu} - p_1^\nu p_2^\mu). \quad (2.127)$$

Summing over all 8 gluons, performing the polarisation sums and multiplying a factor $\frac{1}{2}$ due

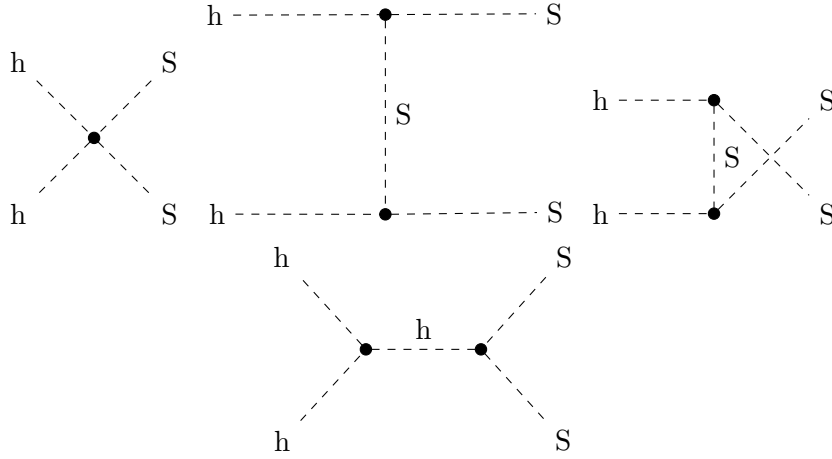


Figure 2.4: Relevant tree-level diagrams for Higgs annihilation into dark matter. In addition to the direct 4-vertex, a s-, t- and a u-channel diagram appear.

to the identical incoming particles, we receive

$$|M_{h \rightarrow gg}|^2 = 16 \cdot 4L_{GGH}^2 s^2 \quad (2.128)$$

$$\Rightarrow \Gamma_{h \rightarrow gg} = \frac{4}{\pi} L_{GGH}^2 \sqrt{s}^3. \quad (2.129)$$

Next, we want to describe the dark matter production from annihilation of the Higgs $hh \rightarrow ss$. There are four contributing tree-level processes, which are pictured in figure 2.4: The direct S, S, h, h four vertex and a s-, t-, and u-channel process. As mentioned above, we can not describe the cross section through decay rates, since certain parts depend not only on s . The matrix elements corresponding to the different diagrams are given below:

$$M_{hh \rightarrow SS}^{direct} = -i\lambda_{hS} \quad (2.130)$$

$$M_{hh \rightarrow SS}^s = -3\lambda_{hS} m_h^2 \frac{i}{s - m_h^2 + im_h \Gamma_h} \quad (2.131)$$

$$M_{hh \rightarrow SS}^t = -\lambda_{hS}^2 v^2(T) \frac{i}{t - m_s^2} \quad (2.132)$$

$$M_{hh \rightarrow SS}^u = -\lambda_{hS}^2 v^2(T) \frac{i}{u - m_s^2} = -\lambda_{hS}^2 v^2(T) \frac{i}{ms^2 - t + 2m_h^2 - s} \quad (2.133)$$

We used that $s + t + u = 2m_s^2 + 2m_h^2$. The above matrix-elements actually depend only on s and the angle θ between the outgoing particles, which can be seen by writing the ingoing and outgoing momenta respectively in the CMS as

$$p_{1,2} = \frac{\sqrt{s}}{2}(1, 0, 0, \pm\beta_1) \quad (2.134)$$

$$p_{3,4} = \frac{\sqrt{s}}{2}(1, 0, \pm\beta_3 \sin \theta, \pm\beta_3 \cos \theta), \quad (2.135)$$

with $\beta_i = \sqrt{s - \frac{4m_i^2}{s}}$. Clearly, in this way it is still $(p_1 + p_2)^2 = (p_3 + p_4)^2 = s$ and $|\vec{p}| = \sqrt{p_0^2 - m^2}$ as it should be. We can write

$$t = (p_1 - p_3)^2 = -(\vec{p}_1 - \vec{p}_3)^2 = -\frac{s}{4}[\beta_1^2 + \beta_3^2 - 2\beta_1\beta_3 \cos \theta]. \quad (2.136)$$

Clearly, this only depends on s and θ . The evaluation of the cross section can be reduced to:

$$\sigma = \int \frac{1}{4F} |\overline{M}|^2 \frac{1}{(2\pi)^2} \frac{d^3 p_3}{2E_3} \delta((p_1 + p_2 - p_3)^2 - m_{DM}^2) \quad (2.137)$$

$$= \frac{1}{4F} \frac{1}{16\pi} \sqrt{1 - 4m_s^2/s} \int_{-1}^1 d \cos \theta |M|^2 \quad (2.138)$$

$$\Rightarrow \sigma v_{\text{Mø}} = \frac{1}{16\pi \frac{1}{s}} \sqrt{1 - 4m_s^2/s} \int_{-1}^1 d \cos \theta |M|^2. \quad (2.139)$$

The integral as well as the t -substitution above were performed using Mathematica [63].

This integration yields

$$\sigma_{hh \rightarrow SS} v_{\text{Mø}} = \frac{1}{16\pi} \frac{1}{s} \beta_S \left[\lambda_{hs}^2 |D_h(s)|^2 2(\Gamma_h^2 m_h^2 + (2m_h^2 + s)^2) \right] \quad (2.140)$$

$$+ \lambda_{hs}^3 16v(T)^2 \frac{|D_h(s)|^2}{s\beta_h\beta_S} (\Gamma_h^2 m_h^2 - 2m_h^4 + m_h^2 s + s^2) \quad (2.141)$$

$$\times \operatorname{arctanh} \left(\frac{s\beta_h\beta_S}{2m_h^2 - s} \right) + \mathcal{O}(\lambda_{hs}^4) \Big]. \quad (2.142)$$

Here, $|D_h(s)|^2 = \frac{1}{(s - m_h^2)^2 + \Gamma_h^2 m_h^2}$ corresponds to the absolute squared of the Higgs propagator. In most publications considering the scalar singlet model, only the inverse cross sections are presented. Due to the additional integration only s-channel processes can be easily compared. However, the λ_{hs}^2 order only consists of the contact and the s-channel diagram, allowing for a comparison. For this order there is a clear correspondence to the result in [53].

2.8 Real Intermediate State problem

The real intermediate state (RIS) problem is a double counting problem which may appear, when s-channel processes are relevant for the particle production in the Boltzmann equation formalism. For a comprehensive review, see for example [11]. Here, we will only give a brief

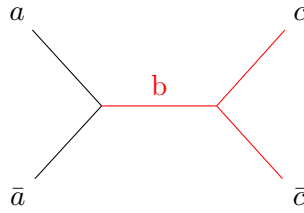


Figure 2.5: Feynman diagram of a $2 \rightarrow 2$ s-channel process. Marked in red is the included decay of the mediator.

overview of the problem.

The real intermediate state problem can be described as follows: If an s-channel particle (for example the particle b in figure 2.5) is produced on-shell, it should be considered a real particle. In this special case, the diagram in figure 2.5 describes the two real processes of annihilation $a\bar{a} \rightarrow b$ and decay $b \rightarrow c\bar{c}$ following after one another.

However, if we assume that the s-channel particle (here b) is in thermal equilibrium, the abundance of the particle is already completely determined by its distribution function f_b . This includes any additional production from such processes as $a\bar{a} \rightarrow b$. Thus, the on-shell part of the $2 \rightarrow 2$ process shown in Figure 2.5 is already included in the decay process marked in red. This leads to a double counting of the resonant part of the s-channel diagram, which should be avoided.

This RIS double counting problem has been known for a long time [64, 65] and has been treated in multiple fields, such as Leptogenesis [66, 67] or Dark Matter [12]. There are multiple approaches to cut out the resonant part of the $2 \rightarrow 2$ process. In the most common procedures, the squared s -channel (Breit-Wigner) propagator is modified, which of course leads to problems, when multiple channels are available [11].

We shall here explain some of the more common procedures, as described in [11]. Perhaps the most straightforward procedure is given by the Standard Real Intermediate State Subtraction (SRS) scheme. Here, the resonance is subtracted as a δ -distribution, which is motivated by the narrow width approximation of a Breit-Wigner propagator:

$$|D_{off}^{SRS}(s)|^2 = |D_{BW}|^2 - \frac{\pi}{m\Gamma}\delta(s - m^2) \quad (2.143)$$

One should be warned that cross sections calculated in the SRS scheme can sometimes be negative, as for example noted in [68].

Another common scheme is the Principal Values Subtraction scheme (PVS), here the resonance is removed by formally taking the principal value of the bare (non-Breit-Wigner) propagator. We have:

$$|D_{off}^{PVS}(s)|^2 = \frac{(s - m^2)^2 - (m\Gamma)^2}{((s - m^2)^2 + (m\Gamma)^2)^2} \quad (2.144)$$

It should be noted that the PVS scheme is equivalent to the SRS scheme up to an order of Γ^2 , as can be seen in the narrow widths approximation [11]. So, they yield the same results for vanishing decay width.

Another commonly used scheme consists of simply taking the real part of the propagator and squaring it. As argued in [11], this is probably just a misunderstanding of the PVS scheme, as square and principle value do not commute. The resulting propagator can be written as:

$$D_{off}^{Real}(s) = \frac{s - m^2}{(s - m^2)^2 + (m\Gamma)^2}, \quad |D_{off}^{Real}(s)|^2 = \frac{(s - m^2)^2}{((s - m^2)^2 + (m\Gamma)^2)^2} \quad (2.145)$$

The above schemes can be implemented numerically by simply replacing the propagator in the matrix elements. For the SRS scheme, it is helpful to explicitly evaluate the δ -distribution over s which occurs in the cross section in equation (2.112), so that we have for Boltzmann statistics as in equation (2.69):

$$\gamma_{DM}^{off} = \gamma_{DM} - \sum_X \frac{1}{(2\pi)^3} \lambda^2 v^2(T) m_h \frac{T}{4} \sqrt{1 - 4 \frac{m_s^2}{m_h^2}} K_1\left(\frac{m_h}{T}\right) \frac{\Gamma_{h \rightarrow X\bar{X}}(m_h^2)}{\Gamma_h} \quad (2.146)$$

$$= \gamma_{DM} - \frac{1}{(2\pi)^3} \lambda^2 v^2(T) m_h \frac{T}{4} \sqrt{1 - 4 \frac{m_s^2}{m_h^2}} K_1\left(\frac{m_h}{T}\right) \quad (2.147)$$

and for Fermi-Dirac statistics as in equation (2.78):

$$\gamma_{DM}^{off} = \gamma_{DM} - \sum_X \frac{1}{8} \frac{1}{(2\pi)^3} \lambda_{hs}^2 v^2(T) \sqrt{\frac{m_h^2 - 4m_s^2}{m_h^2 - 4m_f^2}} F(m_h^2, m_f, m_f) \frac{\Gamma_{h \rightarrow X\bar{X}}(m_h^2)}{\Gamma_h} \quad (2.148)$$

where $F(m_h^2, m_f, m_f)$ is the integral over fermi functions as in equation (2.85) and X are the considered particle species. The decay widths can be canceled, if one only considers Boltzmann statistics, since the rest of the term is independent of the particle species.

Other procedures to deal with the RIS problem, which do not directly modify the propagator, exist. For example in [10, 69] instead the width occurring in the Breit-Wigner propagator is modified. A different approach to avoid the RIS problem is given in [12] and relies on the application of holomorphic cutting rules.

We will just mention these approaches here for the sake of completeness, but will not elaborate

them further. Instead, we will see in the next chapter that a different formulation of the Boltzmann equation, which avoids the RIS problem, may be derived from thermal field theory in the Keldysh-Schwinger formulation. As we will see in section 3.6, the approach from thermal field theory will lead to surprisingly similar expressions as the approach in [12], when examined at finite order.

3 Dark Matter freeze-in in non-equilibrium field theory

The discussions in chapter 2 were based entirely on zero-temperature QFT. However, at high temperatures or densities such a description of physics is highly dubious. First approaches to a finite temperature field theory (FTFT) stem from many body physics (e.g. [15]), where this problem is of course more prevalent. However, by now, the use of FTFTs or non-equilibrium field theory has also spread to particle physics, finding use for example in high temperature QCD to study the Quark-gluon plasma [16] [17] [18], neutrino physics [19] [20], or dark matter physics [13].

More to the point of this thesis, the Boltzmann equation approach discussed in chapter 2 relies on scattering matrix elements which are calculated in vacuum QFT. While there exist multiple approaches to enhance the predictability of the Boltzmann equation in a high temperature context, all of these treat the temperature effectively (e.g. thermal masses, [10] [48]). Additionally, we had seen in section 2.8, that the Boltzmann equation formalism exhibits a problem, when real intermediate states are kinematically allowed.

In this chapter, we will first give a brief overview over different FTFT formalisms in section 3.1, before we give an introduction to the closed time path (CTP) formalism. In section 3.3, we will start from the Kadanoff-Baym equations in the CTP formalism to derive an evolution equation for particle densities, which naturally arises from the equation and only depends on the self energy of the particle. This allows us to calculate the DM relic densities, while properly treating thermal effects. Additionally, the calculations also do not exhibit the RIS problem [11]. We will use section 3.4 and section 3.5 to explicitly calculate the occurring self energies and show in section 3.6 that the terms we found in the Boltzmann equation formalism can be recovered in this formalism. The CTP will also allow us to calculate thermal contributions to the Higgs effective potential in section 3.7.

The overview over different schemes and the derivation of basic properties of the CTP formalism will follow the descriptions in [18], [70] and [14].

3.1 FTFT formalisms

Throughout the years, three majorly different formulations have been developed for thermal field theories. We will give a brief general overview over these different approaches:

The first considerations of field theory at finite temperature and density are due to Matsubara [15] in the 50s. His imaginary time (or Matsubara) formalism is based on the observation that a Boltzmann distribution $e^{-\beta H}$ can be related to the QM time evolution e^{-itH} by considering $i\beta$ as a purely imaginary time. The resulting Green's functions take imaginary time arguments (or live in Euclidean space), hence the name. In Fourier space, the Matsubara formalism is defined on discrete complex energies which have to be summed over for internal lines. Multiple resummation schemes have been developed for this purpose. However, the definition on discrete energies poses a problem in the calculations of dynamical quantities, where continuous real-time valued Green's functions are necessary. While the Matsubara formalism has some problems due to its unphysical treatment of time and energy, it is well suited to treat static properties, such as thermodynamic potentials.

Much better suited for treating dynamical and non-equilibrium properties is the so called real-time (or Keldysh-Schwinger) formalism which was developed by Keldysh [71] and Schwinger [72]. Here, the time-ordering of propagators is along complex time-paths. Inside certain bounds, these time paths can be chosen freely, which also allows for real time components of the path. Real-time formalisms and especially the so-called closed-time-path (CTP) formalism will be discussed in more detail below. It should already be noted here that the real-time formalisms generally lead to a doubling of the degrees of freedom compared to vacuum QFT.

There, furthermore, exists thermo-field dynamics (TFD) [73, 74] or Umezawa formalism which is an operator formalism for finite temperature field theory, which can be formulated on the C^* formulation of Quantum statistical mechanics. It has been shown in [75], that TFD and the real time formalism are equivalent formulations. We will not dive deeper into thermo-field dynamics in this thesis, but it should be noted that the doubling of the degrees of freedom observed in the Keldysh-Schwinger formalism can be consistently derived from TFD and is not just an artifact of the former theory.

3.2 Introduction to the time path formalism

In the following we will give a short introduction to the real-time formalism and show some derivations of key expressions. The section is mostly based on [18] and [14].

One of the core assumptions of the S-matrix formalism of vacuum QFT is the existence of asymptotically free states at the time-like infinities, which are evolved through time. However, this notion is not well suited to describe the situation in a (dense or hot) medium where a particle will not be truly free. Instead it is more useful, to calculate expectation values of operators, with respect to (statistical) density matrices $\rho(t)$

$$\langle \mathcal{O} \rangle_\rho(t) = \text{Tr}[\rho(t)\mathcal{O}]. \quad (3.1)$$

However, now we want to describe expectation values of operators not just with dependence on time but also temperature. We had noticed earlier that there is a formal analogy between the time evolution in QM e^{-itH} and the Boltzmann distribution $e^{-\beta H}$. In fact, the density matrix for a system in equilibrium at constant temperature (canonical ensemble) is given as $\rho(T) = \frac{1}{Z}e^{-\beta H}$. As such, it makes sense to formally allow to evaluate equation (3.1) at complex time arguments to include thermal effects.

To do so, one typically defines a complex time path C along which time may be parametrised as $t = z(v)$ with v monotonically increasing. This parametrisation also allows to easily define time path δ - and θ -distributions

$$\theta_C(t - t') = \theta(v - v') \quad \delta_C(t - t') = \left(\frac{\partial z}{\partial v} \right)^{-1} \delta(v - v') \quad (3.2)$$

and to extend functional derivation along the contour:

$$\frac{\delta j(x)}{\delta j(x')} = \delta_C(t - t') \delta^{(3)}(\vec{x} - \vec{x}') \quad (3.3)$$

We will for now leave the specific contour arbitrary and only switch to the specific case of the CTP contour later. Additionally, to keep things simple, we will only discuss the following derivations for a real scalar field ϕ whose dynamics are governed by a time-independent Hamiltonian H .

To make statements about observables of ϕ , one is ultimately interested in the calculation of correlation functions which may be written along C as

$$G_C(x_1, \dots, x_N) = \langle T_C(\phi(x_1) \dots \phi(x_N)) \rangle. \quad (3.4)$$

Here, T_C is the time ordering along C which is defined as the standard time ordering with

respect to the parametrisation v or more formal in terms of the time-path θ -function:

$$T_C(\phi(x)\phi(x')) = \theta_C(t-t')\phi(x)\phi(x') + \theta_C(t'-t)\phi(x')\phi(x) \quad (3.5)$$

As is quite common in path integral formulations of QFT, one seeks a generating functional $Z_C(j)$ such that arbitrary correlation functions can be generated from its functional derivatives:

$$G_C(x_1, \dots, x_N) = \frac{1}{Z_C(j=0)} \frac{\delta^N Z_C(j)}{i\delta j(x_1) \dots i\delta j(x_N)} \Big|_{j=0} \quad (3.6)$$

We additionally demand that $Z_C(j=0)$ is the partition function. In equilibrium:

$$Z_C(j=0) = Z(\beta) = \text{Tr}(\exp(-\beta H)).$$

A solution for $Z_C(j)$ is then

$$Z_C(j) = \text{Tr} \left[\rho(t_i) T_C \exp \left(i \int_C d^4 x j(x) \phi(x) \right) \right] Z_C(0), \quad (3.7)$$

where $\rho(t_i)$ is the density matrix at some initial time which is completely determined in equilibrium. C must be chosen to pass through all complex time points which are of relevance to the correlation functions we wish to evaluate. It is then clear, that equation (3.7) fulfills equation (3.6) by taking functional derivatives:

$$\frac{1}{Z(\beta)} \frac{\delta^N Z_C(\beta, j)}{i\delta j(x_1) \dots i\delta j(x_N)} \Big|_{j=0} = \text{Tr}[\rho(t_i) T_C(\phi(x_1) \dots \phi(x_N))] \quad (3.8)$$

Typically, one wants to represent the generating functional equation (3.7) through a path integral. To do so, let $|\phi(\vec{x}); t\rangle$ be the eigenstate of the field operator $\phi(t, \vec{x})$ in the Heisenberg picture and $|\phi\rangle = \otimes_{\vec{x} \in \mathbb{R}^3} |\phi(\vec{x})\rangle$. Since these states form a complete set, we may write the trace of an operator as

$$\text{Tr}(\mathcal{O}) = \int [d\phi] \langle \phi; t | \mathcal{O} | \phi; t \rangle, \quad (3.9)$$

where the measure could either be defined as $[d\phi] = \prod_{\vec{x} \in \mathbb{R}^3} d\phi(\vec{x})$ or better be interpreted as an integral of a functional with respect to the field configurations ϕ , as it is done in [58]. It is then also conventional to write the measure as $\mathcal{D}\phi$. Typically one hides awkward normalisation factors in the measure $\mathcal{D}\phi$. We may write the generating functional as

$$Z_C(\beta, j) = Z(0) \int \mathcal{D}\phi \langle \phi; t | \rho(t_i) T_C \exp \left(i \int_C d^4 x j(x) \phi(x) \right) | \phi; t \rangle. \quad (3.10)$$

For a general $\rho(t_i)$, there is some difficulty in choosing a proper parametrization of the density

matrix (see for example [14]). However, we may for now just consider the equilibrium case $Z(0)\rho(\beta) = e^{-\beta H}$. We may treat $e^{-\beta H}$ as a time evolution into the imaginary direction and write

$$Z_C(\beta, j) = \int \mathcal{D}\phi \langle \phi; t | e^{-\beta H} | \phi; t \rangle T_C \exp\left(i \int_C d^4x j(x)\phi(x)\right) \quad (3.11)$$

$$= \int \tilde{\mathcal{D}}\phi \exp\left(i \int_t^{t-i\beta} d^4x \mathcal{L}(x)\right) \exp\left(i \int_C d^4x j(x)\phi(x)\right) \quad (3.12)$$

$$= \int \tilde{\mathcal{D}}\phi \exp\left(i \int_C d^4x \mathcal{L}(x) + j(x)\phi(x)\right). \quad (3.13)$$

In principle the evaluation of $\langle \phi; t | e^{-\beta H} | \phi; t \rangle$ will yield an extra path integral as in [58]. However it will only provide a normalisation factor which we may absorb in $\tilde{\mathcal{D}}\phi$ and we will drop the tilde over the measure again in the following. The last step in equation (3.13) holds, for time paths C going from initial time t to final time $t-i\beta$ and for periodic boundary conditions $\phi(x^0, \vec{x}) = \phi(x^0 - i\beta, \vec{x})$. We left out the explicit mention of the time ordering along C , as it is already guaranteed by the form of the exponential. For the above steps, it is furthermore required, that the Lagrangian density does not contain any derivative interactions.

In the free theory it is simply $\mathcal{L} = -\frac{1}{2}\phi(x)(\square_x + m^2)\phi(x)$ and it is helpful to perform the path integral. To do so, we will follow the procedure applied in [58]. With a redefinition $\phi'(x) = \phi(x) - i \int_C d^4y G_F(x-y)j(y)$, where G_F is a Green's function of the free theory, and the use of the Gaussian integral, we can write

$$Z_C^F(\beta, j) = \int \mathcal{D}\phi \exp\left(i \int_C d^4x \left[-\frac{1}{2}\phi(x)(\square_x + m^2)\phi(x) + j(x)\phi(x)\right]\right) \quad (3.14)$$

$$= \int \mathcal{D}\phi \exp\left(i \int_C d^4x \left[-\frac{1}{2}\phi'(x)(\square_x + m^2)\phi'(x) + \frac{i}{2} \int_C d^4y j(y)G_F(x-y)j(y)\right]\right) \quad (3.15)$$

$$= \mathcal{N} \exp\left[-\frac{1}{2} \int_C d^4x d^4y J(x)G_F(x-y)J(y)\right]. \quad (3.16)$$

Here, \mathcal{N} is simply a normalisation constant, which stems from the Gaussian integral, but has no further impact.

At this point we may wonder what time contour C we should actually choose. We have seen above that the time path should run from t to $t-i\beta$. But we also set out with the goal of calculating real time Green's functions, so our time-path should include the real axis. The standard choice for the finite temperature time path is shown in figure 3.1. This time path starts at some far negative time $t_i \rightarrow -\infty$, runs into the far future $t_f \rightarrow \infty$ and loops around

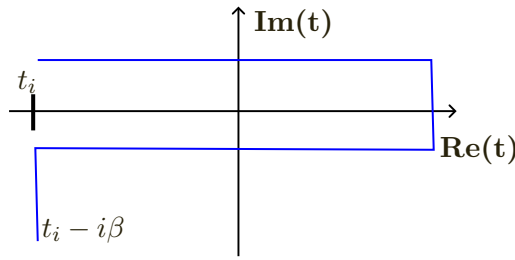


Figure 3.1: Real time path.

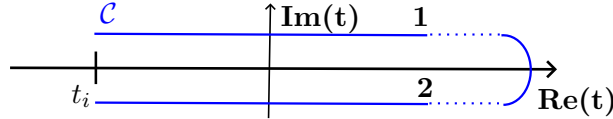


Figure 3.2: Keldysh-Schwinger (or closed) time path.

to $t_i - i\beta$. It is argued in [18] that the generating functional can be factorised into parts parallel and orthogonal to the real axis, when the limit $t_i \rightarrow -\infty$ is taken. Then the paths orthogonal to the real axis only provide a multiplicative constant and may be ignored. It is then common to choose the Keldysh-Schwinger time path shown in figure 3.2 instead, which can also be used in non-equilibrium scenarios.

3.2.1 Equilibrium propagators in the CTP formalism

The goal of this section is the derivation of the equilibrium propagators as well as some useful relations. We had defined the contour C for complex time arguments above. However, as the contour now consists of two branches, which both run along the real time axis, it is useful and common to instead describe the path via real time $t \in]-\infty, \infty[$ and label the two branches with causal indices $a = 1, 2$. With this labeling, equation (3.16) turns into

$$Z_C^F(\beta, j) = \mathcal{N} \exp \left[-\frac{1}{2} \int_{-\infty}^{\infty} d^4x d^4y J_a(x) G_F^{ab}(x-y) J_b(y) \right]. \quad (3.17)$$

Here, the sum over $a, b = 1, 2$ should be understood implicitly. We can already see that in terms of real time t there will be not just one, but four propagators

$$i\Delta_F^{ab}(x_1, x_2) = \frac{1}{Z_C^F(j=0)} \frac{\delta^2 Z_C^F(j)}{i\delta j_a(x_1) i\delta j_b(x_2)} \Big|_{j=0} = G_{ab}^F(x_1, x_2), \quad (3.18)$$

which may be conveniently written as a matrix. It should be noted that this is a sign of the doubled degrees of freedom in the thermal field theory. The fields living on branch 2 should hereby be interpreted as a kind of ghost field, which should not occur for external/physical particles [18].

To make notation simpler later on, we will also define some additional propagators and self energies as linear combinations of the causal ones. First, we will introduce the spectral density

$$\rho(x, y) = \Delta^-(x, y) = i\Delta^{21}(x, y) - i\Delta^{12}(x, y). \quad (3.19)$$

We can then introduce the retarded and advanced Green's functions, which can also be expressed through the causal Green's function we already know as

$$\Delta^R(x, y) = \theta(x^0 - y^0)\rho(x, y) = \Delta^{11} - \Delta^{12} = \Delta^{21} - \Delta^{22} \quad (3.20)$$

$$\Delta^A(x, y) = -\theta(y^0 - x^0)\rho(x, y) = \Delta^{11} - \Delta^{21} = \Delta^{12} - \Delta^{22}. \quad (3.21)$$

here, we suppressed the spacial coordinates of the causal Green's functions.

We will also introduce the hermitian and anti-hermitian (or spectral) propagators as:

$$\Delta^{\mathcal{H}} = \frac{1}{2}(\Delta^R + \Delta^A) = \frac{1}{2}(\Delta^{11} - \Delta^{22}) \quad (3.22)$$

$$\Delta^{\mathcal{A}} = \frac{i}{2}(\Delta^R - \Delta^A) = \frac{1}{2}\rho \quad (3.23)$$

Before we derive the explicit form of the free propagators, it is useful to derive a relation for general expectation values of two operators in equilibrium, which uses the cyclic property of the trace:

$$\langle \mathcal{O}_1(t_1)\mathcal{O}_2(t_2) \rangle_\beta = \frac{1}{Z} \text{Tr} \left[e^{-\beta H} \mathcal{O}_1(t_1)\mathcal{O}_2(t_2) \right] = \frac{1}{Z} \text{Tr} \left[e^{\beta H} e^{-\beta H} \mathcal{O}_2(t_2)e^{-\beta H} \mathcal{O}_1(t_1) \right] \quad (3.24)$$

$$= \langle \mathcal{O}_2(t_2)\mathcal{O}_1(t_1 + i\beta) \rangle_\beta \quad (3.25)$$

This is called the Kubo-Martin-Schwinger (KMS) relation, which can of course be applied for the scalar propagators as

$$\Delta^{21}(x, y) = \Delta^{12}((\vec{x}, t + i\beta), y). \quad (3.26)$$

Even more useful is the Fourier transformed version:

$$\Delta^{21}(p) = e^{\beta p_0} \Delta^{12}(p) \quad (3.27)$$

The KMS relation also allows us to write a relation for the Wightman functions and the

spectral propagator from equation (3.23), which will be useful later:

$$i\Delta^<(p) = i\Delta^{12}(p) = 2f_-(p_0)\Delta^{\mathcal{A}}(p) \quad (3.28)$$

$$i\Delta^>(p) = i\Delta^{21}(p) = 2(1 + f_-(p_0))\Delta^{\mathcal{A}}(p) \quad (3.29)$$

Here, the distribution functions should be understood as their continuation for potential negative values of p_0 . One should note that the derivation above was done explicitly assuming an equilibrium situation. In fact, it has been argued in [76] that the KMS relation cannot hold outside of equilibrium. Luckily, for this thesis, we will need the KMS relation mainly for propagators or self energies of the Higgs boson, which is assumed to be in equilibrium with the standard model.

Now, we may derive the explicit form of the free propagators. We could solve for the Green's functions by applying proper boundary conditions as in [18, 14]. Instead, we will here follow the approach in [70] and write the free scalar boson propagators as an expectation value of ordered fields, which may be developed in terms of their creation and annihilation operators as

$$i\Delta^>(x_1, x_2) = \langle \phi(x_1)\phi(x_2) \rangle \quad (3.30)$$

$$= \int d\Pi_{k_1} d\Pi_{k_2} \langle a_{k_1} a_{k_2}^\dagger \rangle e^{ik_2 x_2 - k_1 x_1} + \langle a_{k_1}^\dagger a_{k_2} \rangle e^{ik_1 x_1 - k_2 x_2} \quad (3.31)$$

$$= \int d\Pi_k (1 + f_-(\omega_k)) e^{-i\omega_k(t_1 - t_2) + i\vec{k}(\vec{x}_1 - \vec{x}_2)} + f_-(\omega_k) e^{i\omega_k(t_1 - t_2) - i\vec{k}(\vec{x}_1 - \vec{x}_2)} \quad (3.32)$$

$$= \int \frac{d^4k}{(2\pi)^4} 2\pi\delta(k^2 - m^2) e^{-k(x_1 - x_2)} \{ [1 + f_-(\omega_k)]\theta(k_0) + f_-(\omega_k)\theta(-k_0) \}. \quad (3.33)$$

This leads to a propagator in momentum space of

$$i\Delta^>(k) = 2\pi\delta(k^2 - m^2)[f_-(|k_0|) + \theta(k_0)] \quad (3.34)$$

$$i\Delta^<(k) = e^{-\beta k_0} i\Delta^>(k) = 2\pi\delta(k^2 - m^2)[f_-(|k_0|) + \theta(-k_0)], \quad (3.35)$$

where we again used the KMS relation to find $\Delta^<$. The diagonal parts of the propagator can then be derived by writing the time ordering with the help of the Wightmann functions as

$$i\Delta^{11}(x_1, x_2) = \theta(t_1 - t_2) i\Delta^>(x_1, x_2) + \theta(t_2 - t_1) i\Delta^<(x_1, x_2) \quad (3.36)$$

$$= \mathcal{F}[2\pi\delta(k^2 - m^2)(f_-(\omega_k) + \theta(t_1 - t_2)\theta(k_0) + \theta(-t_1 + t_2)\theta(-k_0))], \quad (3.37)$$

where \mathcal{F} indicates a Fourier transformation. Then, taking the Fourier-transform with respect to the relative coordinate $r = x_1 - x_2$ and using the convolution theorem, as well as $\mathcal{F}(\theta(r_0)) =$

$\frac{i}{k_0 + i\epsilon} \delta(\vec{k})$ we can write

$$\mathcal{F}[\mathcal{F}(2\pi\delta(k^2 - m^2)\theta(k_0))\theta(r_0)] = \delta(k^2 - m^2)\theta(k_0) \odot \frac{i}{k_0 + i\epsilon} \delta^{(3)}(\vec{k}) \quad (3.38)$$

$$= \int dq_0 \frac{1}{2\omega_k} \sum_{+,-} \delta(k_0 - q_0 \pm \omega_k) \theta(k_0 - q_0) \frac{i}{q_0 + i\epsilon} \quad (3.39)$$

$$= \frac{1}{2\omega_k} \frac{i}{k_0 - \omega_k + i\epsilon}. \quad (3.40)$$

Here, \odot refers to the convolution. And in the same way it is

$$\mathcal{F}[\mathcal{F}(2\pi\delta(k^2 - m^2)\theta(-k_0))\theta(-r_0)] = -\frac{1}{2\omega_k} \frac{i}{k_0 + \omega_k - i\epsilon}. \quad (3.41)$$

This ultimately allows us to write equation (3.37) as

$$i\Delta^{11}(k) = 2\pi\delta(k^2 - m^2)f_-(\omega_k) + \frac{1}{2\omega_k} \left(\frac{i}{k_0 - \omega_k + i\epsilon} - \frac{i}{k_0 + \omega_k - i\epsilon} \right) \quad (3.42)$$

$$= \frac{i}{k^2 - m^2 + i\epsilon} + 2\pi\delta(k^2 - m^2)f_-(\omega_k). \quad (3.43)$$

The $i\Delta^{22}(k)$ propagator is just the complex conjugate of the above, which allows us to write all the free scalar boson propagators as

$$i\Delta^{11}(k) = \frac{i}{k^2 - m^2 + i\epsilon} + 2\pi\delta(k^2 - m^2)f_-(\omega_k) = (i\Delta^{22})^*(k) \quad (3.44)$$

$$i\Delta^>(k) = 2\pi\delta(k^2 - m^2)[f_-(|k_0|) + \theta(k_0)] \quad (3.45)$$

$$i\Delta^<(k) = 2\pi\delta(k^2 - m^2)[f_-(|k_0|) + \theta(-k_0)]. \quad (3.46)$$

Of course, we will also need to describe fermions in this thesis and thus require the form of their FTFT propagators. We will not repeat the derivation for fermions and instead just give the propagators here. The free fermionic propagators in equilibrium are given as [77, 20]:

$$i\mathcal{S}^{11}(k) = \frac{i(\not{k} - m)}{k^2 - m^2 + i\epsilon} - 2\pi(\not{k} - m)\delta(k^2 - m^2)f_+(|k_0|) = (i\mathcal{S}^{11}(k))^* \quad (3.47)$$

$$i\mathcal{S}^>(k) = -2\pi(\not{k} - m)\delta(k^2 - m^2)[f_+(|k_0|) - \theta(-k_0)] \quad (3.48)$$

$$i\mathcal{S}^<(k) = -2\pi(\not{k} - m)\delta(k^2 - m^2)[f_+(|k_0|) - \theta(k_0)] \quad (3.49)$$

Now, that we derived the free equilibrium propagators, it is a good time to talk about the Feynman rules of the CTP formalism. They are as in vacuum with the exception of the causal indices corresponding to the two different branches of the time-contour. As such, there are also two different vertices corresponding to the 1 and 2 branch. Since the 1 indices correspond

to the “normal” time ordering, they behave as vacuum vertices, while the 2 type vertices receive an extra factor of -1 due to their inverse time-ordering. Vertices only ever correspond to one type and vertices of type a and b have to be connected by a D^{ab} propagator. Internal indices need to be summed over. Additionally, real external fermions have to connect to type 1 vertices.

We should also make a brief comment about renormalization in the CTP formalism. The next sections will contain multiple loop integrals. One might be worried, that UV divergent terms, which require renormalization appear in this context. However, it has been shown in [78] that all temperature dependent UV divergences will cancel in each order of perturbation theory. Consequently, renormalization at zero temperature will already assure finite results at all other temperatures. Due to the equivalence between the real-time formalism and TFD shown in [75], this also holds for the calculations performed in this thesis. So, we do not need to perform any renormalization in this thesis and can instead rely on the renormalization in the zero temperature standard model.

3.2.2 The Dyson-Schwinger and Kadanoff-Baym equations

In the above, we only derived the free propagators. However, in a realistic scenario, these can at best hold as an approximation for the full propagators. The goal of this section is to find equations which fully determine the form of the full propagators. We will also derive the Kadanoff-Baym equations which are evolution equations for the propagators and will be of larger importance in section 3.3.

First we should note, that we have no guarantee that the full propagators only depend on the relative coordinate. As such, we will introduce the Wigner-transformation for functions depending on two real-space coordinates x, y to still describe expressions in momentum space:

$$G(k, x) = \int d^4r e^{ikr} G(x + \frac{r}{2}, x - \frac{r}{2}) \quad (3.50)$$

It should be noted that the Wigner transformation reduces to the ordinary Fourier transformation, if G in fact only depends on the relative coordinate.

We will also give the following useful identity for Wigner-transformations of convolutions:

$$A \odot B(k, x) = e^{-i\odot} \{A(k, x)\} \{B(k, x)\} \quad (3.51)$$

Here, \odot is the Moyal-product, which is defined as

$$\odot\{A\}\{B\} = \frac{1}{2}(\partial_x A \partial_k B - \partial_k A \partial_x B). \quad (3.52)$$

Of course, the exponentiation of the Moyal-product should be understood as a series expansion. We will not proof this identity, but instead refer to the original derivation in [79].

We can now turn to the defining equations for the full propagator. There are multiple approaches to derive the Dyson-Schwinger equations. In [14, 13] the DS eq. are derived from 1-PI or 2-PI effective actions. However, we can also take the approach in [70]: Because the Feynman rules at finite temperature have the same structure as those in vacuum QFT, we can write an analogous Dyson series for the full propagator as

$$G^{ab}(x, y) = G_F^{ab}(x, y) - i \int d^4x' d^4y' [G_F(x, x') \Pi(x', y') G(y', y)]^{ab}. \quad (3.53)$$

Here the full propagator is described in terms of the free propagator $G_F^{ab}(x, y)$ and in terms of self-energies Π^{cd} . The brackets $[...]^{ab}$ should be understood as a sum over all internal thermal indices, such that the outer indices correspond to a, b . It should be noted that extra factors of (-1) might occur in the summation due to internal 2-type vertices. Taking the Wigner-transform of this equation, yields

$$G^{ab}(k, x) = G_F^{ab}(k, x) - [iG_F(k, x) \Pi(k, x) G(k, x)]^{ab}. \quad (3.54)$$

The above can be seen by performing the transformation and using $e^{ikr} = e^{ikr_1} e^{ikr_2} e^{ikr_3}$, with $r_1 = x + \frac{r}{2} - x'$, $r_2 = x' - y'$, $r_3 = y' - x + \frac{r}{2}$, as well as a shift of the integral to the r_i . Equation (3.54) is also called the Dyson-Schwinger equation of thermal field theory and completely characterises the full propagator. A formal solution may be constructed by multiplying with the inverse propagators to get

$$(G^{ab}(k, x))^{-1} = (G_F^{ab}(k, x))^{-1} + i\Pi^{ab}(k, x). \quad (3.55)$$

While the above are commonly cited forms of the Dyson-Schwinger equation, we should start from equation (3.53) to derive the Kadanoff-Baym (KB) equations. In the case of scalar bosons, we write $G^{ab} = i\Delta^{ab}$ and due to the definition of the free propagator as the Green's function, it is $(\partial_x^2 + m^2)\Delta_F^{ab}(x, y) = (-1)^a \delta_{ab} \delta(x - y)$. Here, an extra factor $(-1)^{a-1}$ is due to the specific definition of the path ordered δ -distributions (equation (3.2)). We can now

multiply equation (3.53) with $-(\partial_x^2 + m^2)$ to receive

$$-(\partial_x^2 + m^2)i\Delta^{ab}(x, y) \quad (3.56)$$

$$\begin{aligned} &= (-1)^{a-1}\delta_{ab}i\delta(x-y) + i \int d^4x' d^4y' (-1)^a \delta_{ac} \delta(x-y) (-1)^{c-1} \Pi^{cd}(x', y') (-1)^{d-1} i\Delta^{db}(y', y) \\ &= (-1)^{a-1}\delta_{ab}i\delta(x-y) + i(-1)^d \int d^4y' i\Pi^{ad}(x, y') i\Delta^{db}(y', y). \end{aligned} \quad (3.57)$$

Here, summation over twice occurring thermal indices should be understood implicitly.

In terms of the linear combinations of propagators in equations (3.21) and (3.23), we may write equation (3.57) for the Wightmann functions as

$$-(\partial_x^2 + m^2)\Delta^< = -\Pi^{12} \odot \Delta^{22} + \Pi^{11} \odot \Delta^{12} \quad (3.58)$$

$$= -\Pi^{12} \odot (\Delta^{22} - \Delta^{12}) + (\Pi^{11} - \Pi^{12}) \odot \Delta^{12} \quad (3.59)$$

$$= \Pi^{12} \odot \Delta^A + \Pi^R \odot \Delta^{12} \quad (3.60)$$

$$= \frac{1}{2}(\Pi^{12} \odot \Delta^A + \Pi^R \odot \Delta^{12}) + \frac{1}{2}(\Pi^A \odot \Delta^{12} + \Pi^{12} \odot \Delta^R + \Pi^{21} \odot \Delta^{12} - \Pi^{12} \odot \Delta^{21}) \quad (3.61)$$

$$= \frac{1}{2}(\Pi^R + \Pi^A) \odot \Delta^{12} + \Pi^{12} \odot (\Delta^A + \Delta^R) + \frac{1}{2}(\Pi^{21} \odot \Delta^{12} - \Pi^{12} \odot \Delta^{21}) \quad (3.62)$$

$$= \Pi^{\mathcal{H}} \odot \Delta^{12} + \Pi^{12} \odot \Delta^{\mathcal{H}} + \frac{1}{2}(\Pi^{21} \odot \Delta^{12} - \Pi^{12} \odot \Delta^{21}). \quad (3.63)$$

Where we used the forms of the propagators in equations (3.21) and (3.23) and $\Delta^A + \Delta^> = \Delta^R + \Delta^<$ and $\Delta^R - \Delta^> = \Delta^A - \Delta^<$. The evolution equation for the other Wightmann function can be derived analogously, leading to the Kadanoff-Baym equations for the scalar boson propagators:

$$-(\partial_x^2 + m^2)\Delta^{\geq} - \Pi^{\mathcal{H}} \odot \Delta^{\geq} - \Pi^{\geq} \odot \Delta^{\mathcal{H}} = \frac{1}{2}(\Pi^{21} \odot \Delta^{12} - \Pi^{12} \odot \Delta^{21}) \quad (3.64)$$

3.3 From the Kadanoff-Baym equations to a time evolution of the DM density

If we look at the equilibrium propagators at finite temperature in equation (3.46), we can see that they depend on the distribution functions of the particle. We have also just derived an evolution equation for the propagators in the form of the Kadanoff-Baym equations in equation (3.64). The goal of this section is to use this to derive an evolution equation for the distribution functions similar to the Boltzmann equation.

This section follows mostly the procedure in [13] and [14]. The main difference is that in the self energies in [13] only particles from the thermal bath appear in loops and the self energy

can be assumed to be proportional to equilibrium distribution functions. This is not the case in our scenario, where the DM self energy again depends on a DM propagator. However, we will show below that kinetic equations can be derived in a more general setting, without any knowledge of the occurring self energies.

By assuming spatial homogeneity and isotropy of the universe, the spatial derivatives drop out of the KB equations and we can write

$$(-\partial_{x,0}^2 - m^2)\Delta^{\cong} - \Pi^{\mathcal{H}} \odot \Delta^{\cong} - \Pi^{\cong} \odot \Delta^{\mathcal{H}} = \frac{1}{2}(\Pi^> \odot \Delta^< - \Pi^< \odot \Delta^>). \quad (3.65)$$

To transform the equation into Wigner space, we may use

$$\int d^4r e^{ikr} \partial_{x,0}^2 \Delta(z + \frac{r}{2}, z - \frac{r}{2}) = \int d^4r e^{ikr} (\frac{1}{2} \partial_{z,0} + \partial_{r,0})^2 \Delta(z + \frac{r}{2}, z - \frac{r}{2}) \quad (3.66)$$

$$= \frac{1}{4} \partial_{z,0}^2 \Delta(k, z) - ik_0 \partial_{z,0} \Delta(k, z) - k_0^2 \Delta(k, z) + \text{boundary terms}. \quad (3.67)$$

The boundary terms can be assumed to be zero for propagators, which vanish at infinity. If we also use equation (3.51), the Kadanoff-Baym equation turns into

$$\begin{aligned} (-\frac{1}{4} \partial_{z,0}^2 + ik_0 \partial_{z,0} + k_0^2 - m^2) \Delta^{\cong}(k) - e^{-i\circ} \{ \Pi^{\mathcal{H}} \} \{ \Delta^{\cong} \} - e^{-i\circ} \{ \Pi^{\cong} \} \{ \Delta^{\mathcal{H}} \} \\ = \frac{1}{2} (e^{-i\circ} \{ \Pi^> \} \{ \Delta^< \} - e^{-i\circ} \{ \Pi^< \} \{ \Delta^> \}). \end{aligned} \quad (3.68)$$

It is $\Delta^{\mathcal{H}}, \Delta^{\mathcal{A}} \in \mathbb{R}$ and also $\Pi^{\mathcal{H}}, \Pi^{\mathcal{A}} \in \mathbb{R}$. From the KMS relations in the form of equation (3.29), we can then also see, that Δ^{\cong} and Π^{\cong} are purely imaginary. If we expand the exponentials and only consider the real part of equation (3.68), we receive a kinetic equation of the propagator:

$$ik_0 \partial_{z,0} \Delta^{\cong}(k) = \frac{1}{2} (\Pi^> \Delta^< - \Pi^< \Delta^>) + \mathcal{O}(\partial_0 \Delta^{\mathcal{H}, \cong}; \partial_0 \Pi^{\mathcal{H}, \cong}) \quad (3.69)$$

As the gradient correction containing temporal derivatives in equation (3.69) are heavily suppressed in a freeze-in scenario [13], we will ignore these terms. The kinetic equation of the propagator is then

$$k_0 \partial_{z,0} i \Delta^{\cong}(k) = -\frac{1}{2} (i \Pi^> i \Delta^< - i \Pi^< i \Delta^>). \quad (3.70)$$

We can translate the above equation, into an evolution equation of the DM density by writing

the off-diagonal thermal DM propagators as

$$i\Delta_{DM}^<(k) = 2\pi\delta(k^2 - m^2)[f_{DM}(|k_0|) + \theta(-k_0)] \quad (3.71)$$

$$i\Delta_{DM}^>(k) = 2\pi\delta(k^2 - m^2)[f_{DM}(|k_0|) + \theta(k_0)]. \quad (3.72)$$

This is of course the equilibrium form, where the equilibrium distribution function has been replaced with the actual distribution. It has been claimed in [77] that this still holds outside of equilibrium. However, further references point to a book which apparently exists only in Chinese. Alternatively, we may assume that the self-coupling of S is large enough and leads to the DM being in equilibrium with itself. Then we can assign a temperature T_{DM} to the DM (which may be different than the standard model temperature). Then we can write the DM propagator as $f_{DM} = f_-(T_{DM}(T))$, where T is the SM temperature, and equation (3.72) still holds.

Integrating this form of the DM propagator allows us to write the DM distribution function as

$$f_{DM}(\omega_k) = \int_0^\infty \frac{dk_0}{\pi} f_{DM}(k) \pi \delta(k_0 - \omega_k) = \int_0^\infty \frac{dk_0}{\pi} i\Delta^<(k) k_0, \quad (3.73)$$

where $\omega_k = \sqrt{|\vec{k}|^2 + m^2}$. We then get an evolution equation for f_{DM} by inserting equation (3.70). In a freeze-in scenario, we can also assume the DM-densities on the RHS to vanish, leaving only the terms depending on θ -functions in the off-diagonal DM propagators. With this, we receive an evolution equation of the DM distribution as

$$\partial_t f_{DM}(\omega_k) = \int_0^\infty \frac{dk_0}{\pi} k_0 \partial_0 i\Delta^<(k) \quad (3.74)$$

$$= \int_0^\infty \frac{dk_0}{\pi} \frac{1}{2} (i\Pi^<i\Delta^> - i\Pi^>i\Delta^<) \quad (3.75)$$

$$= \int_0^\infty \frac{dk_0}{\pi} \frac{1}{2} i\Pi^< 2\pi\delta(k^2 - m^2)\theta(k_0) \quad (3.76)$$

$$= \frac{i\Pi^<(\omega_k, \vec{k})}{2\omega_k}. \quad (3.77)$$

Note, that in contrast to the procedure in [13] no assumption of the shape of Π^{\geq} was necessary in the above calculations. By integrating over the 3-momentum, we then receive an evolution equation for the DM density:

$$\partial_t n_s(t) = \int \frac{d^3k}{(2\pi)^3} \frac{i\Pi^<(\omega_k, \vec{k})}{2\omega_k} = \frac{1}{4\pi^2} \int d|\vec{k}| \frac{|\vec{k}|^2}{\omega_k} i\Pi^<(\omega_k, |\vec{k}|) \quad (3.78)$$

For now all our calculations took place in Minkowski space. However, the expansion of the universe has a relevant impact on the dark matter density in our universe. As we have seen in section 2.4, considering instead a FLRW metric of the universe leads to the familiar form of the LHS of the Boltzmann equation. The RHS of equation (3.78) is instead not impacted by the change of metric, as it is already covariant. This leads to the following evolution equation in the FLRW metric:

$$\partial_t n_s(t) - 3Hn_s(t) = \frac{1}{4\pi^2} \int d|\vec{k}| \frac{|\vec{k}|^2}{\omega_k} i\Pi^<(\omega_k, |\vec{k}|) := \gamma_{DM} \quad (3.79)$$

Here we called the RHS of the equation γ_{DM} in formal analogy to the scattering term in the Boltzmann equation (2.23). As in the case of the Boltzmann equation, we will actually calculate the DM density by solving the equation

$$\frac{dY}{dx} = \frac{1}{Hsx} \left(1 + \frac{1}{3} \frac{d \ln(h_{eff})}{dT} \frac{m}{x} \right) \frac{1}{4\pi^2} \int d|\vec{k}| \frac{|\vec{k}|^2}{\omega_k} i\Pi^<(\omega_k, |\vec{k}|). \quad (3.80)$$

3.4 Dark matter self energy

As we had seen in the previous section, the evolution equations for the dark matter densities are completely determined by the dark matter self energy. So, to determine the DM relic densities, we will use this and the following section to determine the self energy. Before we start the calculations of any self energies, it should be briefly mentioned, that there exist two different conventions in the literature. The additional factors of $(-1)^{a+b}$ of the external causal indices can either be considered part of the self energy (as in [14][20]) or counted as a separate factor (as in [13]). We will here follow the latter convention, as we already implicitly used it in the derivation of the Kadanoff-Baym equations. The reader should be aware that factors of (-1) might pop up in comparison to some literature, depending on the chosen conventions.

Now for the calculation of the self energy, we will ignore the quartic coupling of Higgs and dark matter, as in the calculations in the Boltzmann equation formalism and focus just on the contributions from the SSh coupling. The self energy is then given by the diagram in figure 3.3 and can be written as

$$i\Pi^{a,b}(p) = \lambda_{hS}^2 v^2(T) \int \frac{d^4k}{(2\pi)^4} i\Delta_S^{ab}(k) i\Delta_h^{ba}(k-p). \quad (3.81)$$

We assume, that the dark matter Wightmann functions can be written as in equation (3.72). Of course, as the momentum is evaluated for both positive as well as negative values, the

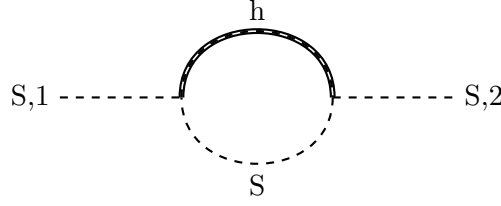


Figure 3.3: Feynman diagram of the dark matter self energy. S is the scalar dark matter and h the Higgs. The double line represents a resummed propagator.

θ -functions assure that a finite contribution remains even under the freeze-in assumption of $f_{DM} \approx 0$. The off-diagonal self-energy is then

$$i\Pi^{12}(p) = \lambda_{hS}^2 v^2(T) \int \frac{d^4 k}{(2\pi)^4} i\Delta_S^{12}(k) i\Delta_h^{21}(k-p) \quad (3.82)$$

$$= \lambda_{hS}^2 v^2(T) \int \frac{d^4 k}{(2\pi)^4} 2\pi \delta(k^2 - m^2) \Theta(-k_0) i\Delta_h^{21}(k-p) \quad (3.83)$$

$$= \lambda_{hS}^2 v^2(T) \int \frac{d^4 k}{(2\pi)^4} 2\pi \frac{1}{2\omega_k} \delta(k_0 \mp \omega_k) \Theta(-k_0) i\Delta_h^{21}(k-p) \quad (3.84)$$

$$= \lambda_{hS}^2 v^2(T) \int \frac{d^3 k}{(2\pi)^3} \frac{1}{2\omega_k} i\Delta_h^{21}(-\omega_k - p_0, \vec{k} - \vec{p}) \quad (3.85)$$

$$= \lambda_{hS}^2 v^2(T) \int \frac{d^3 k}{(2\pi)^3} \frac{1}{2\omega_k} i\Delta_h^{12}(\omega_k + p_0, \vec{p} - \vec{k}) \quad (3.86)$$

$$= \lambda_{hS}^2 v^2(T) \int \frac{d^3 k}{(2\pi)^3} \frac{1}{2\omega_k} i\Delta_h^{12}(\omega_k + p_0, \vec{p} + \vec{k}). \quad (3.87)$$

Where we used that $\Delta^{12}(p) = \Delta^{21}(-p)$. This can be seen from the KMS relation in the form of equation (3.29) and the fact that $1 + f_-(k_0) = -f_-(-k_0)$. We also use that the spectral propagator should be assymmetric with respect to energy. We also switched $\vec{k} \rightarrow -\vec{k}$ in the last step. We cannot fully solve this integral analytically due to the, at this point, unknown propagator of the Higgs. However, we can reduce the integral to a two dimensional one by using the fact that $\Delta_h^{12}(\omega_k + p_0, \vec{p} + \vec{k})$ in fact only depends on $|\vec{p} + \vec{k}|$, not $\vec{p} + \vec{k}$ (which will be motivated later). Additionally, we use the substitution $q_i = p_i + k_i$, $d^3 k = d^3 p$. The self energy is then

$$i\Pi^{12}(p) = \lambda_{hS}^2 v^2(T) \int \frac{d^3 q}{(2\pi)^3} \frac{1}{2\omega_k} i\Delta_h^{12}(\omega_k + p_0, |\vec{q}|) \quad (3.88)$$

$$= \lambda_{hS}^2 v^2(T) \int_0^\infty \frac{d|\vec{q}|}{(2\pi)^2} \int_{-1}^1 d\cos\theta \frac{|\vec{q}|^2}{2\omega_k} i\Delta_h^{12}(\omega_k + p_0, |\vec{q}|), \quad (3.89)$$

with $\omega_k = \sqrt{|\vec{p}|^2 + |\vec{q}|^2 - 2|\vec{p}||\vec{q}|\cos\theta + m_s^2}$. A further analytic simplification is not possible at this stage.

As already indicated in figure 3.3 we should not just consider the bare Higgs propagator,

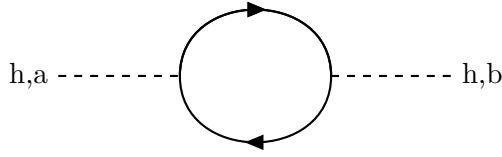


Figure 3.4: Feynman diagram considered for the Higgs self energy.

but all loop corrections leading to the resummed propagator. As we will see in section 3.6, the loop corrections significantly add to the self energy and allow us to recover certain terms we might already expect from the semi classical Boltzmann equation. We may ignore loop corrections to the dark matter propagator, because the coupling between dark matter and standard model must be feeble, as a key ingredient of a freeze-in scenario.

Starting from the Dyson-Schwinger equation (3.54) one may derive the resummed propagator Δ^{12} of the Higgs in terms of the hermitian $\Pi^{\mathcal{H}}$ and spectral self energies $\Pi^{\mathcal{A}}$ of the Higgs to be [13]

$$i\Delta^{12}(k) = \frac{2\Pi^{\mathcal{A}}}{(k^2 - m^2 - \Pi^{\mathcal{H}})^2 + (\Pi^{\mathcal{A}})^2} f_-(k_0, T). \quad (3.90)$$

Here, f_- is a Bose distribution and the self energies $\Pi^{\mathcal{H}}$ and $\Pi^{\mathcal{A}}$ are defined as linear combinations of the causal self energies in analogy to equation (3.23). It should be noted, that the resummed propagator sometimes appears with an extra sign of (-1) in the literature, which depends on the convention for the self energies as mentioned above.

Of course, to determine the Higgs propagator, we now need to calculate the thermal self energies of the Higgs. This will be done in the next section.

3.5 Thermal Higgs self energies

We will here only consider insertions of fermionic self energy loops as in figure 3.4. As we will see in section 3.6, this corresponds to only considering the decay and fermion annihilation terms in the semi-classical Boltzmann equation.

3.5.1 Wightmann self energy

With the KMS relations in the form of equation (3.29), which holds for self energies in the same way it does for propagators, we can express the antihermitian Higgs self energy as:

$$\Pi_h^{\mathcal{A}} = \frac{i}{2} f_-^{-1} \Pi_h^{\mathcal{H}} \quad (3.91)$$

So, we only need to calculate $\Pi_h^<$ to determine the antihermitan SE. Writing down the causal self energy, we receive an extra factor of (-1) due to the fermion loop. It is then

$$i\Pi_h^{ab} = - \sum_f \frac{(y_{h,ff})^2}{2} N_{C,f} \int \frac{d^4k}{(2\pi)^4} \text{Tr} \left\{ i\cancel{\mathcal{S}}_f^{ab}(k) i\cancel{\mathcal{S}}_f^{ba}(k-p) \right\} \quad (3.92)$$

$$\Rightarrow i\Pi_h^< = - \sum_f \frac{(y_{h,ff})^2}{2} N_{C,f} \int \frac{d^4k}{(2\pi)^4} \text{Tr} \left\{ i\cancel{\mathcal{S}}_f^<(k) i\cancel{\mathcal{S}}_f^>(k-p) \right\}. \quad (3.93)$$

Here $y_{h,ff}$ is the Yukawa coupling, $N_{C,f}$ is the number of colours and $\cancel{\mathcal{S}}_f^{ab}$ is the thermal propagator of the fermion, which is slashed here to indicate its matrix structure.

To actually calculate the self energy, we will partially use the procedure and a couple of techniques employed in [13]. Instead of using the Fermion propagators given in equation (3.49), we can use that under formal extension of the Fermi distribution to negative energies it is $f_+(-k_0) = 1 - f_+(k_0)$ and we may then rewrite the propagators as

$$\cancel{\mathcal{S}}_f^<(k) = -2\pi\delta(k^2 - m_f^2)(\not{k} + m_f)f_+(k_0)\text{sgn}(k_0) \quad (3.94)$$

$$\cancel{\mathcal{S}}_f^>(q) = 2\pi\delta(q^2 - m_f^2)(\not{q} + m_f)(1 - f_+(q_0))\text{sgn}(q_0). \quad (3.95)$$

Then the trace over the propagators turns into

$$\begin{aligned} \text{Tr} \left\{ i\cancel{\mathcal{S}}_f^<(k) i\cancel{\mathcal{S}}_f^>(k-p) \right\} &= -4\pi^2 \text{Tr} \left\{ (\not{k} + m)(\not{k} - \not{p} + m) \right\} f_+(k_0)(1 - f_+(k_0 - p_0)) \\ &\quad \text{sgn}(k_0)\text{sgn}(k_0 - p_0)\delta(k^2 - m_f^2)\delta((k-p)^2 - m_f^2) \end{aligned} \quad (3.96)$$

$$\begin{aligned} &= -16\pi^2(k^2 - k \cdot p + m_f^2)f_+(k_0)(1 - f_+(k_0 - p_0)) \\ &\quad \text{sgn}(k_0)\text{sgn}(k_0 - p_0)\delta(k^2 - m_f^2)\delta((k-p)^2 - m_f^2). \end{aligned} \quad (3.97)$$

Using the identity [13]

$$f_-^{-1}(p_0)f_+(k_0)(1 - f_+(k_0 - p_0)) = 1 - f_+(k_0) - f_+(p_0 - k_0) \quad (3.98)$$

as well as the substitution

$$d^4k \rightarrow \frac{1}{2|\vec{p}|} d\phi dk_0 d(p \cdot k) dk^2 \quad (3.99)$$

the antihermitian self-energy turns into

$$\begin{aligned} \Pi_h^A(p) &= 4\pi^2 \sum_f (y_{h,ff})^2 N_{C,f} \int \frac{d^4k}{(2\pi)^4} \delta(k^2 - m_f^2) \delta((k-p)^2 - m_f^2) (k^2 - k \cdot p + m_f^2) \\ &\quad \text{sgn}(k_0) \text{sgn}(k_0 - p_0) [1 - f_+(k_0) - f_+(p_0 - k_0)] \end{aligned} \quad (3.100)$$

$$\begin{aligned} &= \frac{1}{8\pi^2 |\vec{p}|} \sum_f (y_{h,ff})^2 N_{C,f} \int d\phi dk_0 d(p \cdot k) dk^2 \delta(k^2 - m_f^2) \delta(k^2 + p^2 - 2p \cdot k - m_f^2) \\ &\quad (k^2 - k \cdot p + m_f^2) \text{sgn}(k_0) \text{sgn}(k_0 - p_0) [1 - f_+(k_0) - f_+(p_0 - k_0)] \end{aligned} \quad (3.101)$$

$$\begin{aligned} &= \frac{1}{8\pi^2 |\vec{p}|} \sum_f (y_{h,ff})^2 N_{C,f} \int d\phi dk_0 d(p \cdot k) \frac{1}{2} \delta(p \cdot k - \frac{1}{2} p^2) (2m_f^2 - k \cdot p) \\ &\quad \text{sgn}(k_0) \text{sgn}(k_0 - p_0) [1 - f_+(k_0) - f_+(p_0 - k_0)] \end{aligned} \quad (3.102)$$

$$\begin{aligned} &= \frac{1}{16\pi^2 |\vec{p}|} \sum_f (y_{h,ff})^2 N_{C,f} \int d\phi dk_0 (2m_f^2 - \frac{1}{2} p^2) \\ &\quad \text{sgn}(k_0) \text{sgn}(k_0 - p_0) [1 - f_+(k_0) - f_+(p_0 - k_0)] \end{aligned} \quad (3.103)$$

$$\begin{aligned} &= \frac{1}{16\pi |\vec{p}|} \sum_f (y_{h,ff})^2 N_{C,f} (4m_f^2 - p^2) \\ &\quad \int dk_0 \text{sgn}(k_0) \text{sgn}(k_0 - p_0) [1 - f_+(k_0) - f_+(p_0 - k_0)]. \end{aligned} \quad (3.104)$$

In reality, the integral over k_0 should not be evaluated over the entirety of \mathbb{R} . The evaluated δ -distributions instead only allow values of k_0 in a limited range. From $\delta(p^2 - 2k \cdot p)$ and $\delta(k^2 - m_f^2)$, we receive the conditions:

$$p_0 k_0 - |\vec{p}| |\vec{k}| \leq \frac{p^2}{2} \leq p_0 k_0 + |\vec{p}| |\vec{k}| \quad (3.105)$$

$$\Rightarrow p_0 k_0 - |\vec{p}| \sqrt{k_0^2 - m_f^2} \leq \frac{p^2}{2} \leq p_0 k_0 + |\vec{p}| \sqrt{k_0^2 - m_f^2} \quad (3.106)$$

$$\Leftrightarrow -|\vec{p}| \sqrt{k_0^2 - m_f^2} \leq \frac{p^2}{2} - p_0 k_0 \leq |\vec{p}| \sqrt{k_0^2 - m_f^2} \quad (3.107)$$

$$\Leftrightarrow \left(\frac{p^2}{2} - p_0 k_0 \right)^2 \leq |\vec{k}|^2 (k_0^2 - m_f^2) \quad (3.108)$$

Solving this equation, yields the solutions

$$k_0^\pm = \frac{1}{2} \left(p_0 \pm |\vec{p}| \sqrt{1 - \frac{4m_f^2}{p^2}} \right). \quad (3.109)$$

This only exists, if $p^2 < 0$ or $p^2 > 4m_f^2$, which might be expected from kinematic constraints. In fact, we are only interested in solutions with positive p^2 since it is defined as a sum of two real particles in equation (3.89) (there it is called q). In that case, it is $p_0 > |\vec{p}|$ and the

square root appearing in equation (3.109) has to be smaller 1. Then it is $0 < k_0 < p_0$ and we have $\text{sgn}(k_0)\text{sgn}(k_0 - p_0) = -1$. This allows us to write

$$\begin{aligned} \Pi_h^A(p) &= \frac{1}{16\pi|\vec{p}|} \sum_f (y_{h,ff})^2 N_{C,f}(p^2 - 4m_f^2) \Theta(p^2 - 4m_f^2) \\ &\quad \times \int_{k_0^-}^{k_0^+} dk_0 [1 - f_+(k_0) - f_+(p_0 - k_0)], \end{aligned} \quad (3.110)$$

which can be solved analytically. To do so, we can employ the substitution $u = e^{\beta k_0} + 1$ to write the integral over a Fermi distribution as

$$\int_{k_0^-}^{k_0^+} dk_0 f_+(k_0) = k_0^+ - k_0^- + \frac{1}{\beta} \ln \left(\frac{e^{\beta k_0^-} + 1}{e^{\beta k_0^+} + 1} \right) \quad (3.111)$$

and then also

$$\int_{k_0^-}^{k_0^+} dk_0 f_+(p_0 - k_0) = k_0^+ - k_0^- + \frac{1}{\beta} \ln \left(\frac{e^{\beta(p_0 - k_0^+)} + 1}{e^{\beta(p_0 - k_0^-)} + 1} \right). \quad (3.112)$$

This allows us, to write the integral appearing in equation (3.110) as

$$\int_{k_0^-}^{k_0^+} dk_0 [1 - f_+(k_0) - f_+(p_0 - k_0)] \quad (3.113)$$

$$= k_0^- - k_0^+ + \frac{1}{\beta} \ln \left(\frac{(e^{\beta k_0^+} + 1)(e^{\beta(p_0 - k_0^-)} + 1)}{(e^{\beta k_0^-} + 1)(e^{\beta(p_0 - k_0^+)} + 1)} \right) \quad (3.114)$$

$$= \frac{1}{\beta} \ln \left(\frac{\cosh\left(\frac{\beta}{2}k_0^+\right) \cosh\left(\frac{\beta}{2}(p_0 - k_0^-)\right)}{\cosh\left(\frac{\beta}{2}k_0^-\right) \cosh\left(\frac{\beta}{2}(p_0 - k_0^+)\right)} \right). \quad (3.115)$$

Where the last step can be seen by writing $e^{\beta k_0} + 1 = 2 \cosh\left(\frac{\beta k_0}{2}\right) e^{\frac{\beta k_0}{2}}$.

In total, the antihermitian self-energy can be evaluated to be

$$\begin{aligned} \Pi_h^A(p) &= \frac{1}{16\pi|\vec{p}|} \sum_f (y_{h,ff})^2 N_{C,f}(p^2 - 4m_f^2) \Theta(p^2 - 4m_f^2) \\ &\quad \times \frac{1}{\beta} \ln \left(\frac{\cosh\left(\frac{\beta}{2}k_0^+\right) \cosh\left(\frac{\beta}{2}(p_0 - k_0^-)\right)}{\cosh\left(\frac{\beta}{2}k_0^-\right) \cosh\left(\frac{\beta}{2}(p_0 - k_0^+)\right)} \right). \end{aligned} \quad (3.116)$$

3.5.2 Hermitian self energy

The Hermitian self energy can be written as $\Pi^{\mathcal{H}} = \frac{1}{2}(\Pi^{11} - \Pi^{22}) = \text{Re}\{\Pi^{11}\}$. And we have

$$i\Pi^{11} = - \sum_f \frac{(y_{h,ff})^2}{2} N_{C,f} \int \frac{d^4k}{(2\pi)^4} \text{Tr}\left\{i\mathcal{S}^{11}(k)i\mathcal{S}^{11}(k+p)\right\}. \quad (3.117)$$

It should be noted that we do not use the same loop-momenta here as in equation (3.93). But it is clear that we can transform the momenta back by a momentum shift $k \rightarrow k - p$. We write the thermal fermion propagator in the form given in equation (3.49):

$$i\mathcal{S}^{11} = \frac{i(\not{p} + m)}{p^2 - m^2 - i\epsilon} - 2\pi(\not{p} + m)\delta(p^2 - m^2)f_+(|p_0|) \quad (3.118)$$

Then, we can already imagine that the self energy can be divided into a vacuum and a thermal part. The vacuum part

$$\Pi_{vac}^{11} = i \sum_f \frac{(y_{h,ff})^2}{2} N_{C,f} \int \frac{d^4k}{(2\pi)^4} \text{Tr}\left\{\frac{i(\not{k} + m)}{k^2 - m^2 + i\epsilon} \frac{i(\not{k} + \not{p} + m)}{(k+p)^2 - m^2 + i\epsilon}\right\} \quad (3.119)$$

is known from vacuum QFT. This part is not relevant here, as it is already absorbed in the mass of the Higgs m_h^2 after renormalization in vacuum QFT. With

$$\text{Tr}\{(\not{k} + m)(\not{k} + \not{p} + m)\} = 4(k^2 + k \cdot p + m^2), \quad (3.120)$$

the thermal part can be written as

$$\begin{aligned} \Pi_T^{11} = & i \sum_f \frac{(y_{h,ff})^2}{2} N_{C,f} \int \frac{d^4k}{(2\pi)^4} 4(k^2 + k \cdot p + m^2) \\ & \left[\frac{-i}{p^2 - m^2 + i\epsilon} 2\pi\delta((k+p)^2 - m^2)f_+(|k_0 + p_0|) \right. \\ & - \frac{i}{(p+k)^2 - m^2 + i\epsilon} 2\pi\delta(k^2 - m^2)f_+(|k_0|) \\ & \left. + 4\pi^2\delta(k^2 - m^2)\delta((k+p)^2 - m^2)f_+(|k_0|)f_+(|k_0 + p_0|) \right]. \quad (3.121) \end{aligned}$$

Here the last line produces a purely imaginary result and consequently is of no interest to us. So, we will only consider the two other parts of the integral. To evaluate them, perform a $k \rightarrow -(k+p)$ shift in the first integral. Since this leaves

$$(k^2 + pk) \rightarrow (k+p)^2 - (k+p)p = k^2 + kp \quad (3.122)$$

invariant, it allows us to write

$$\text{Re}\{\Pi^{11}\} = \sum_f \frac{(y_{h,ff})^2}{2} N_{C,f} \int \frac{d^4k}{(2\pi)^4} 16\pi \frac{k^2 + kp + m^2}{(k+p)^2 - m^2 + i\epsilon} f_+(|k_0|) \delta(k^2 - m^2) \quad (3.123)$$

$$= \sum_f \frac{(y_{h,ff})^2}{2} N_{C,f} 4[p_\mu K^\mu + 2m^2 \bar{K}]. \quad (3.124)$$

Here, we used that k is on-shell, which allows us to write $k^2 = m^2$. We use here the notations for the thermal integrals employed in [20]. The scalar thermal integral can be calculated to be

$$\bar{K} = \int \frac{d^4k}{(2\pi)^3} \frac{f_+(|k_0|) \delta(k^2 - m^2)}{(k+p)^2 - m^2 + i\epsilon} \quad (3.125)$$

$$= \int \frac{d|\vec{k}|}{(2\pi)^2} d\cos\theta 2 \frac{|\vec{k}|^2}{2\omega_k} f_+(\omega_k) \sum_{\pm} \frac{1}{p^2 \pm 2\omega_k p_0 - 2|\vec{p}||\vec{k}| \cos\theta} \quad (3.126)$$

$$= \sum_{\pm} \int \frac{d|\vec{k}|}{(2\pi)^2} d\cos\theta \frac{|\vec{k}|}{2\omega_k |\vec{p}|} f_+(\omega_k) \frac{1}{\frac{p^2 \pm 2\omega_k p_0}{2|\vec{k}||\vec{p}|} - \cos\theta} \quad (3.127)$$

$$= \sum_{\pm} \int \frac{d|\vec{k}|}{(2\pi)^2} \frac{|\vec{k}|}{2\omega_k |\vec{p}|} f_+(\omega_k) \ln \left[\frac{p^2 \pm 2\omega_k p_0 + 2|\vec{p}||\vec{k}|}{p^2 \pm 2\omega_k p_0 - 2|\vec{p}||\vec{k}|} \right] \quad (3.128)$$

$$= \int \frac{d\omega_k}{(2\pi)^2} \frac{1}{2|\vec{p}|} f_+(\omega_k) l_1(\omega, p), \quad (3.129)$$

where we write as in [20]

$$l_1(\omega, p) = \ln \left[\frac{(p^2 + 2|\vec{k}||\vec{p}|)^2 - 4p_0^2 \omega^2}{(p^2 - 2|\vec{k}||\vec{p}|)^2 - 4p_0^2 \omega^2} \right] \quad (3.130)$$

by evaluating the sum of the logarithms. Equation (3.129) is the same result one might receive from a contraction $g_{\mu\nu} K^{\mu\nu}$ of the tensorial integral from [20]. The contraction of the vector integral given in [20] will be:

$$p_\mu K^\mu = \frac{1}{8\pi^2 |\vec{p}|} p_0 \int d\omega \omega l_2(\omega, p) f_+(\omega) - \frac{1}{16\pi^2 |\vec{p}|} \int d\omega [p^2 l_1(\omega, p) + 2\omega p_0 l_2(\omega, p) - 8|\vec{k}||\vec{p}|] f_+(\omega) \quad (3.131)$$

$$= \frac{1}{16\pi^2 |\vec{p}|} \int d\omega [-p^2 l_1(\omega, p) + 8|\vec{k}||\vec{p}|] f_+(\omega) \quad (3.132)$$

In total, the Hermitian self energy can be written as

$$\Pi^{\mathcal{H}} = \sum_f (y_{h,ff})^2 N_{C,f} \frac{1}{|\vec{p}| 8\pi^2} \int d\omega [(4m^2 - p^2) l_1(\omega, p) + 8|\vec{k}||\vec{p}|] f_+(\omega). \quad (3.133)$$

This remaining integral has to be solved numerically. However, we may employ an approximation to receive an analytical result. The so called hard thermal loop (HTL) approximation [80] assumes that the integral can be divided into hard ($\mathcal{O}(\pi T)$) and soft ($\mathcal{O}(gT)$) scales and that the integral is dominated by such momenta k which are much larger than all other mass scales. This allows us to neglect all masses and expand in momenta p/k . As in [20], we have in HTL approximation $l_1(\omega, p) = -2\frac{|\vec{p}|}{|\vec{k}|}$. Additionally, we can write $(4m^2 - p^2)/|\vec{k}| \approx (4m^2 - p^2)/\omega_k \approx 0$. The only remaining integral is then

$$\int d\omega |\vec{k}| f(\omega) \approx \int d\omega \frac{\omega}{e^{\beta\omega} + 1} = \int du \frac{1}{\beta^2} \frac{u}{e^u + 1} \quad (3.134)$$

$$= T^2 F_1(0) \Gamma(2) = T^2 \eta(2) \Gamma(2) = \frac{T^2 \pi^2}{12}. \quad (3.135)$$

Here, F is a Fermi integral, Γ a gamma function and η a Dirichlet function. Then the hermitian self-energy in the HTL limit becomes

$$\Pi_{\text{HTL}}^{\mathcal{H}} = \sum_f (y_{l,ff})^2 N_{C,f} \frac{1}{8\pi^2} \left[\frac{2}{3} \pi^2 T^2 \right] = \sum_f (y_{l,ff})^2 N_{C,f} \frac{T^2}{12}. \quad (3.136)$$

So, in HTL approximation, the hermitian self-energy just leads to a thermal correction to the mass of the particle $m_T \propto T^2$. This is expected for thermal mass corrections, both from dimensional analysis, as well as from similar calculations (e.g. [81]).

We should note that, as argued in [13], the HTL approximation is not well motivated in the context of DM freeze-in. In this context, a majority of DM production will happen at scales $p \approx T \approx m_s$ and then $k \approx p$. The HTL approximation is here not very well justified. However, for the ease of numerical calculation, we will use both the HTL approximation and the full self energies in the numerical calculations. As we will see later, the two procedures yield surprisingly similar results.

3.6 DM Production from multiple orders

In the past sections, we have built a procedure to calculate the dark matter production in the CTP formalism and calculated the necessary self energies. However, one might wonder how the calculations in the CTP formalism relate to the terms of the semi-classical Boltzmann equation we considered in chapter 2. This will also allow us, to identify the difference to the calculations in chapter 2. To do so, we will expand the Higgs propagator to different loop orders. This is a reasonable approach, as can be seen by sketching the associated Feynman diagrams of the self energies and cutting along the occurring delta distributions as shown in figure 3.5. The two cuts we show there, correspond to the absolute squared matrix element

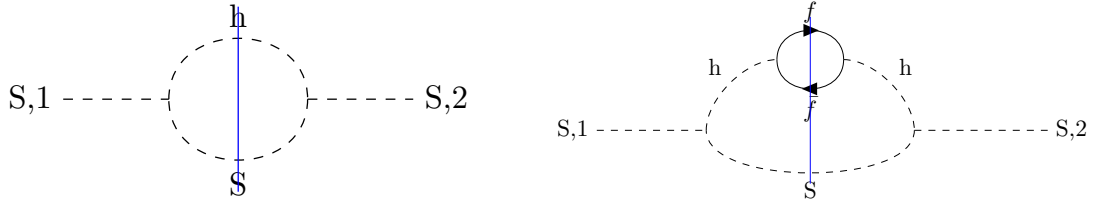


Figure 3.5: Feynman diagrams for the DM self energy with a bare Higgs propagator (left) and the Higgs propagator at 1-loop order (right). Cutting along the blue lines reproduces the squared Matrixelements for the $h \rightarrow SS$ decay process on the left and the $f\bar{f} \rightarrow SS$ process on the right. It should be noted, that depending on the summation of internal indices of the right diagram, there will be additional diagrams with different cuts.

for the decay process and the $2 \rightarrow 2$ process.

3.6.1 Decay terms from bare propagators

At first we will just use the bare Higgs propagator as it is given in equation (3.46) in the evaluation of the DM SE. Using the form of the DM self energy (equation (3.89)), the collision term (equation (3.79)) can then be written as

$$\gamma_{DM} = \int \frac{d^3p}{(2\pi)^3} \frac{i\Pi^<(\omega_p, \vec{p})}{2\omega_p} \quad (3.137)$$

$$= \lambda_{h,s}^2 v^2 \int d\Pi_p \frac{d^4k}{(2\pi)^4} i\Delta_s^{12}(k) i\Delta_h^{21}(k-p) \quad (3.138)$$

$$= \lambda_{h,s}^2 v^2 \int d\Pi_p \frac{d^4k}{(2\pi)^4} 4\pi^2 \delta((k-p)^2 - m_h^2) \delta(k^2 - m_{DM}^2) \\ [f_-(|k_0 - \omega_p|) + \Theta(k_0 - \omega_p)] [f_{DM}(|k_0|) + \Theta(-k_0)] \quad (3.139)$$

$$= \lambda_{h,s}^2 v^2 \int d\Pi_p d\Pi_k \frac{d^4q}{(2\pi)^4} (2\pi)^4 \delta^{(4)}(q - (p-k)) 2\pi \delta((p-k)^2 - m_l^2) f_-(\omega_p + \omega_k) \quad (3.140)$$

$$= \int d\Pi_p d\Pi_k d\Pi_q (2\pi)^4 \delta^{(4)}(q - (p+k)) f_-(\omega_q) 2|M|^2. \quad (3.141)$$

We have used in the second to last equation, that $f_{DM} \approx 0$ and we receive only one solution for $\delta(k^2 - m_{DM}^2)$ which also fullfills the $\theta(-k_0)$. We also performed an extra $k \rightarrow -k$ shift in the last step. In the above, $|M|^2 = \frac{1}{2} \lambda_{h,s}^2 v^2$ is the squared matrix element occurring in the decay process and the factor of 2 also appears in the Boltzmann equation, as there are two final dark matter particles in the decay process. So, the DM production from decay of the Higgs or mediator particle is reproduced in the thermal self energy with bare propagators, as we might expect from figure 3.5. Next, we will look at higher orders of the self energy to identify the $2 \rightarrow 2$ terms.

3.6.2 1-loop self energy and $2 \rightarrow 2$ scattering

If we want to write the scattering term on the order of the 1-loop Higgs propagator, we need to first identify the Higgs propagator at this order. By inserting one free propagator on the RHS of the Dyson-Schwinger equation (3.54), we can see that the 1-loop correction of the scalar propagator can be written as

$$-i\Delta_{1\text{-loop}}^{ab} = \sum_{c,d} (-1)^{c+d} i\Delta_0^{ac} i\Pi_0^{cd} i\Delta_0^{db}. \quad (3.142)$$

The additional factors (-1) stem from the potential internal 2-type indices. The Wightmann propagator, which is relevant in the present case, can then be written as

$$-i\Delta_{1\text{-loop}}^{12} = i\Delta_0^{11} i\Pi_0^{11} i\Delta_0^{12} + i\Delta_0^{12} i\Pi_0^{22} i\Delta_0^{22} - i\Delta_0^{11} i\Pi_0^{12} i\Delta_0^{22} - i\Delta_0^{12} i\Pi_0^{21} i\Delta_0^{12} \quad (3.143)$$

$$= 2 \operatorname{Re}\{i\Delta_0^{11} i\Pi_0^{11} i\Delta_0^{12}\} - i\Delta_0^{11} i\Pi_0^{12} i\Delta_0^{22} - i\Delta_0^{12} i\Pi_0^{21} i\Delta_0^{12}, \quad (3.144)$$

where we used that the first two terms are complex conjugates of each other, due to the relations of the diagonal propagators and self energies ($i\Delta^{11} = (i\Delta^{22})^*$).

Because the thermal propagators contain δ -distributions in the momentum, most of the terms above force the Higgs propagator to be on-shell. To identify the term belonging to $2 \rightarrow 2$ scattering, we are only searching for the off-shell part. The only term with an off-shell contribution is

$$i\Delta_0^{11} i\Pi_0^{12} i\Delta_0^{22} = |i\Delta_0^{11}|^2 i\Pi_0^{12} \quad (3.145)$$

$$= \left[\frac{1}{(p^2 - m_l^2)^2 + \epsilon^2} + 4\pi^2 \delta(p^2 - m^2) \delta(p^2 - m^2) f_{-}(|p_0|)^2 \right] i\Pi_0^{12}. \quad (3.146)$$

We will deal with the pinch singularity appearing in the second term later and will for now concern ourselves only with the first term which we will also call Δ_{off}^{12} . Using equations (3.78) and (3.87) allows us to write the collision term as

$$\gamma_{DM}^{\text{off}} = \int \frac{d^3p}{(2\pi)^3} \frac{i\Pi^<(\omega_p, \vec{p})}{2\omega_p} \quad (3.147)$$

$$= \lambda_{h,s}^2 v^2 \int d\Pi_p \frac{d^4k}{(2\pi)^4} i\Delta_s^{12}(k) i\Delta_{\text{off}}^{21}(k-p) \quad (3.148)$$

$$= \lambda^2 v^2 \int d\Pi_p d\Pi_k i\Delta_{\text{off}}^{12}(\omega_k + p_0, \vec{p} + \vec{k}). \quad (3.149)$$

Plucking in Δ_{off}^{12} and using equation (3.104), we can write

$$= \lambda^2 v^2 \int d\Pi_p d\Pi_k \frac{1}{(s - m_h^2)^2} i\Pi_h^{12} \quad (3.150)$$

$$= -\lambda^2 v^2 \int d\Pi_p d\Pi_k \frac{1}{(s - m_h^2)^2} \frac{y_{hff}^2}{2} \int \frac{d^4 v}{(2\pi)^4} 16\pi^2 \delta(v^2 - m_f^2) \delta((v - q)^2 - m_f^2) \\ [f_+(|v_0|) - \Theta(-v_0)][f_+(|v_0 - q_0|) - \Theta(v_0 - q_0)](v^2 - v \cdot q + m_f^2), \quad (3.151)$$

where we wrote $q = p + k$. Due to the occurring δ -distributions, we can already see, as in equation (3.109), that it must be $0 \leq v_0 \leq q_0$, which allows us to drop the occurring θ -functions. If we write the second ingoing momentum as $u = q - v = p + k - v$, we may write

$$s = (p + k)^2 = (v + u)^2 = v^2 + u^2 + 2vu = 2m_f^2 + 2vu \quad (3.152)$$

$$\iff vu = \frac{s}{2} - m_f^2 \quad (3.153)$$

and thus

$$v^2 - vq + m_f^2 = -vu + m_f^2 = -\frac{1}{2}(s - 4m_f^2). \quad (3.154)$$

We may then write the scattering term as

$$\gamma_{DM}^{off} = \lambda^2 v^2 \int d\Pi_p d\Pi_k d\Pi_v \frac{1}{(s - m_h^2)^2} \frac{y_{hff}^2}{2} 16\pi \\ f_+(\omega_v) \delta((v - q)^2 - m_f^2) f_+(|\omega_v - q_0|) \frac{1}{2}(s - 4m_f^2) \quad (3.155)$$

$$= \lambda^2 v^2 y_{hff}^2 \int d\Pi_p d\Pi_k d\Pi_v \frac{1}{(s - m_h^2)^2} 4\pi \frac{d^4 u}{(2\pi)^4} (2\pi)^4 \delta^{(4)}(u + v - p - k) \\ f_+(\omega_v) \delta((v - q)^2 - m_f^2) f_+(|\omega_v - q_0|) (s - 4m_f^2) \quad (3.156)$$

$$= \int d\Pi_p d\Pi_k d\Pi_v d\Pi_u 2|M|^2 (2\pi)^4 \delta^{(4)}(u + v - p - k) f_+(\omega_v) f_+(\omega_u). \quad (3.157)$$

With $|M|^2 = \lambda^2 v^2 \frac{y_{hff}^2}{2} \frac{1}{(s - m_h^2)^2} (s - 4m_f^2)$ the matrix element of the $2 \rightarrow 2$ process and the factor 2 also appears in the Boltzmann equation, as the process is weighted twice, due to two external dark matter particles. So, the result corresponds to the $2 \rightarrow 2$ term of the Boltzmann equation, with some slight deviation: No width occurs in the denominator of $|M|^2$. The width in the vacuum theory stems from the fully resummed propagator, which considers all loop-orders. As such, it can be expected that it only occurs after full resummation in the FTFT approach used here. It should be noted that we only receive the $2 \rightarrow 2$ DM production process here, due to our assumption that $f_{DM} \approx 0$ and the resulting kinematic constraints.

Without this assumption, we would also receive terms from the rotated diagrams ($2 \rightarrow 2$ DM annihilation and scattering).

3.6.3 Cancellation of the pinch singularities and additional finite contributions

As we had seen, in the previous section, multiple terms appear in the 1-loop propagator, which contain two δ -distributions with the same argument. This leads to so called pinch singularities, which are unphysical. So, we need to show, that these terms in fact cancel out among each other. Writing down all remaining 1-loop corrections to the scalar propagators, we find

$$[i\Delta_0^{11}i\Pi_0^{12}i\Delta_0^{22}]_{on} = 4\pi^2\delta(p^2 - m^2)\delta(p^2 - m^2)f_-(|p_0|)^2i\Pi^{12} \quad (3.158)$$

$$i\Delta_0^{12}i\Pi_0^{21}i\Delta_0^{12} = 4\pi^2\delta(p^2 - m^2)\delta(p^2 - m^2)[f_-(|p_0|) + \Theta(-p_0)]^2i\Pi^{21} \quad (3.159)$$

$$\begin{aligned} 2\operatorname{Re}\{i\Delta_0^{11}i\Pi_0^{11}i\Delta_0^{12}\} &= -\operatorname{Re}\left\{\frac{1}{p^2 - m^2 + i\epsilon}4\pi\delta(p^2 - m^2)\right\}[f_-(|p_0|) + \Theta(-p_0)]\operatorname{Im}\{i\Pi^{11}\} \\ &\quad + 8\pi^2\delta(p^2 - m^2)\delta(p^2 - m^2)f_-(|p_0|)[f_-(|p_0|) + \Theta(-p_0)]\operatorname{Re}\{i\Pi^{11}\}. \end{aligned} \quad (3.160)$$

To show that the pinch-singularities in the above terms cancel, we can use

$\operatorname{Re}\{i\Pi^{11}\} = -\operatorname{Im}\{\Pi^{11}\} = -\frac{i}{2}(\Pi^{12} + \Pi^{21})$. Then the prefactors of the pinch singularities in $[i\Delta_0^{11}i\Pi_0^{12}i\Delta_0^{22}]_{on}, i\Delta_0^{12}i\Pi_0^{21}i\Delta_0^{12}$ and the second term in $2\operatorname{Re}\{i\Delta_0^{11}i\Pi_0^{11}i\Delta_0^{12}\}$ combine to

$$\begin{aligned} &4\pi^2[f_-(|p_0|)i\Pi^{12} + [f_-(|p_0|) + \Theta(-p_0)]^2i\Pi^{21} - f_-(|p_0|)[f_-(|p_0|) + \Theta(-p_0)](i\Pi^{12} + i\Pi^{21})] \\ &= -4\pi^2\Theta(-p_0)f_-(|p_0|)i\Pi^{12} + 4\pi^2\Theta(-p_0)[f_-(|p_0|) + \Theta(-p_0)]i\Pi^{21}. \end{aligned} \quad (3.161)$$

This of course cancels for $p_0 > 0$. For $p_0 < 0$ we can use the KMS relation for self energies given in equation (3.27), to write

$$[f_-(|p_0|) + 1]i\Pi^{21} = [f_-(|p_0|) + 1]ie^{-p_0/T}\Pi^{12} = \left(\frac{e^{-p_0/T}}{e^{p_0/T} - 1} + e^{-p_0/T}\right)i\Pi^{12} \quad (3.162)$$

$$= \frac{1}{e^{p_0/T} - 1}i\Pi^{12} = f_-(|p_0|)i\Pi^{12}. \quad (3.163)$$

So, the pinch singularities also vanish for $p_0 < 0$. For the cancellation of pinch singularities and the correspondence with the KMS relation, see also [76]. While [76] argues that the procedure does not hold for scenarios outside of equilibrium, the cancellation of pinch singularities here happens due to properties of the Higgs self energies. Since the Higgs is assumed to be in thermal equilibrium with the SM, our procedure described above remains consistent.

There is only the first term of $2\operatorname{Re}\{i\Delta_0^{11}i\Pi_0^{11}i\Delta_0^{12}\}$ left to evaluate. One might be afraid, that this term also exhibits a pinch singularity. However, we can show that the singularity lies

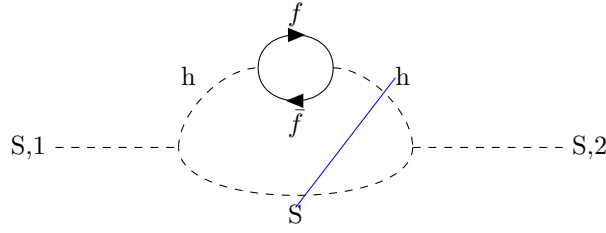


Figure 3.6: 1-loop self energy diagram, with a cut corresponding to the last correction found on the 1-loop order. As we can see, the diagram corresponds to a mixing of the tree-level decay term (on the right of the cut) and the 1-loop correction of the decay term (on the right of the cut).

completely in the imaginary part and only a finite part remains. To do so, use the identity [18]

$$\frac{1}{x + i\epsilon} \delta(x) = -\frac{1}{2} \delta'(x) - i\pi (\delta(x))^2 \quad (3.164)$$

which can be derived from a Gaussian representation of the delta distribution. As we can see, the pinch singularity created by the δ^2 term lies only in the imaginary part, which we are not interested in here. To understand the derivative of the delta distribution occurring in the real part, we can use partial integration:

$$\int \delta'(x) f(x) dx = [\delta(x) f(x)]_{-\infty}^{\infty} - \int dx \delta(x) f'(x) \quad (3.165)$$

The remaining contribution to the propagator can then be written as

$$2 \operatorname{Re}\{i\Delta_0^{11} i\Pi_0^{11} i\Delta_0^{12}\}_{finite} = -2\pi\delta(p^2 - m^2) \frac{\partial}{\partial(p^2 - m^2)} \times [f_-(|p_0|) + \Theta(-p_0)] \operatorname{Re}\{\Pi^{11}\}. \quad (3.166)$$

By comparing this with the diagrammatic approach taken in [12], we can immediately see that this remaining term belongs to a higher order correction to the decay term corresponding to the product of the tree-level and the one-loop matrix element, as we can also guess from the corresponding diagram in figure 3.6.

3.7 Temperature dependent Higgs potential

As discussed earlier in this thesis, one of the main properties of the freeze-in process, in contrast to freeze-out, is its reliance on effects at higher temperature. Thus, a detailed description of such a process should account for as many temperature dependent effects as possible.

As already seen in Section 2.3, the coupling between our dark matter singlet and the standard model depends on the temperature scale, with the hhS coupling becoming only possible after the electroweak symmetry breaking. However, the electroweak phase transition (EWPT) is not an instantaneous transition from the symmetric phase to the current state of the universe, instead the vacuum expectation value of the Higgs and with it the generated masses should shift from 0 at the EWPT to its current value continuously.

To consistently describe the coupling between our dark matter candidate S and the standard model, which depends on $v(T)$, as well as the occurring standard model masses, we need to describe the temperature dependence of the Higgs VEV and mass.

In [10] and [49] following the procedure in [21], the same problem is approached by defining an effective T -dependent Higgs potential. The 1-loop contribution of this Higgs potential are defined by the zero temperature and temperature dependent interactions with the standard model. Then, the VEV $v(T)$ and mass $m_h(T)$ are derived by calculating the minimum and second derivative, evaluated at the minimum of the potential.

While this approach certainly yields results, there are some conceptual issues: For once in [10] and [49] only contributions from t , W and Z loops are considered in the 1-loop potential. However, as stated in [21], this is only a good approximation for small masses of the Higgs $m_h < m_W$, which is of course not compatible with current experimental observations.

One might be tempted to take the potential from [10] and [49] and add additional terms for the scalar Higgs as described in [21]. However, this leads to complications. In the most obvious case, the squared mass of the Higgs will take on negative values outside of the physical minimum, leading to a complex potential. This is also mentioned in [82]. In a more subtle vein, the effective potential is not actually (and cannot be) gauge invariant. However, physical quantities derived from it have to be. With the above procedure, this is not generally the case, as discussed in [82], [83] and [84]. And, while some gauge dependence on the VEV might be expected, a gauge dependence of the Higgs mass, as seen in [85], is not acceptable, because it is a direct observable.

As for example mentioned in [82], [83], [84] or [86], the cause of both such problems (complex potentials and additional gauge dependence) stems from the use of inconsistent perturbation schemes. Despite all this, a perturbative scheme is necessary. Any non-perturbative scheme to evaluate temperature dependent potentials would probably rely on lattice calculations, as suggested in [10]. However, one should make sure that terms are sorted by their importance,

which is not necessarily given in a naive sorting by loop order.

To do so, we will follow the procedure in [84], [22] or [23], using an expansion in the gauge couplings e, g, g' . We will also assume that the selfcoupling $\lambda \propto e^2$, leading to a second order phase transition. Additionally, we should keep in mind that at large temperatures it might be $T \approx 1/g$ or greater. Consequently, to get a consistent perturbation, we should let factors of temperature and gauge couplings cancel for the evaluation of perturbation order. It is thus consistent to only consider the tree-level zero-temperature contribution as well as the 1-loop thermal field theory part. It has also been argued in [23], that the zero temperature 1-loop part, which is also called the Coleman-Weinerg potential, should be considered as a g^4 contribution and will be ignored here. Additionally we can safely ignore all contributions which might be generated by our dark matter particle S due to its feeble coupling.

The tree-level standard model Higgs potential is of course given as

$$V_0(\phi) = -\frac{1}{2}m^2\phi^2 + \frac{\lambda}{4}\phi^4 \quad (3.167)$$

$$m_0^2 = 3\lambda v^2 - m^2. \quad (3.168)$$

To receive analytic results for the temperature dependent VEV and Higgs mass, one might be inclined to use a high temperature expansion. For more details on this approach see appendix A.3. However, it turns out that the resulting values for mass and VEV are not reasonable in the temperature regime we are interested in. This might be expected, as the EWSB only happens on a similar scale to the zero temperature Higgs mass and a relevant portion of the DM production happens at even lower temperatures.

So, we will use the full thermal 1-loop potential. We will here only calculate the effect on the Higgs potential which is created through the self interactions of the Higgs. The calculations for further particles are analogous and can be found in [21]. The self interaction of the Higgs adds some additional subtlety, which we need to address here.

We use, as in [21] that the derivative of the 1-loop Higgs potential may be described by a tadpole diagram. For the self-interactions of the Higgs, this allows us to write in the CTP

resulting 1-loop correction to the effective potential is then

$$V_{1,h}^T = \frac{T}{2\pi^2} \int d|\vec{p}||\vec{p}|^2 \log\left(1 - e^{-\beta\omega_p}\right) \Theta(|\vec{p}|^2 + m_h(\phi)^2) \quad (3.177)$$

$$= \frac{T^4}{2\pi^2} \int_0^\infty dx x^2 \log\left(1 - e^{-\sqrt{x^2 + m_h^2/T^2}}\right) \Theta(x^2 + m_h^2(\phi)T^2). \quad (3.178)$$

The corrections from top, W- and Z-boson are taken from [21], so that the total 1-loop thermal potential can be written as

$$\Delta V_1^T = \frac{T^4}{2\pi^4} \left[\sum_{i=W,Z} n_i J_B(m_i^2(\phi)/T^2) + n_t J_F(m_t^2(\phi)/T^2) + 1 \tilde{J}_B(m_h^2(\phi)/T^2) \right], \quad (3.179)$$

with $n_t = -12$, $n_W = 6$ and $n_Z = 3$, as well as

$$J_B(m^2/T^2) = \int_0^\infty dx x^2 \log\left(1 - e^{-\sqrt{x^2 + m^2/T^2}}\right) \quad (3.180)$$

$$J_F(m^2/T^2) = \int_0^\infty dx x^2 \log\left(1 + e^{-\sqrt{x^2 + m^2/T^2}}\right) \quad (3.181)$$

and \tilde{J}_B includes the extra Θ in the integral as above. The effect of all lighter particles is negligible and will be ignored.

Having found a temperature dependent expression for the Higgs potential, we can now describe the temperature dependent VEV $v(T)$ by numerical minimisation of the effective potential $V_{\text{eff}}(T) = V_0 + \Delta V_1^T$. However, there remains the question of how to consistently derive the mass of the Higgs and how to treat m_h appearing in the temperature dependent potential. The tree-level expression for the Higgs mass $m_h^2 = 3\lambda\phi^2 - m^2$ can only hold close to the zero temperature VEV of $v = 246,22$ GeV and will even yield negative m_h^2 values for small values of the field ϕ . This is clearly unphysical. Instead, one could derive the mass as a second derivative of the potential. However, as mentioned before, there might be a problem with gauge dependence associated with such a procedure. Additionally, using the tree-level mass as input for the potential creates another problem. The potential will exhibit a kink at $\phi = \frac{v_0}{\sqrt{3}}$, where m_h^2 changes sign. If this kink is close to the minimum (which happens around $T = 135,4$ GeV in the present case) it will have a large and clearly unphysical influence on the second derivative of the potential and thus the derived mass of the Higgs.

As we can see above, it is clearly not a good idea, to insert the tree-level mass in the Higgs-potential and then derive a Higgs mass through a second derivative. Instead, we will take an iterative approach. First, we will take into account only the t , W and Z contributions to the

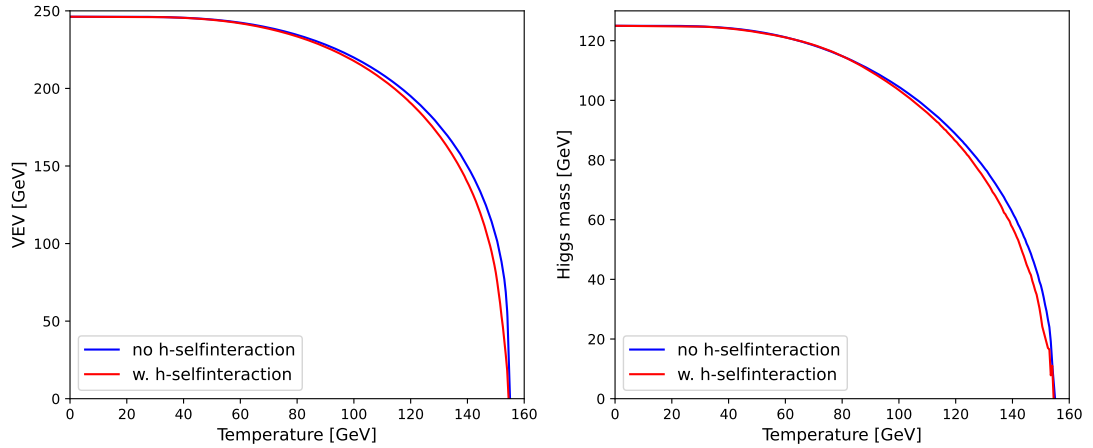


Figure 3.7: Numerical calculated VEV (left) and mass (right) of the Higgs as a function of temperature. In red is the calculation taking under account t , V and W loops. In blue additionally the Higgs loop is taken into account.

Higgs potential. These do not depend on m_h . By numerical evaluation of the minimum and second derivative, we can then derive v and m_h^2 at different temperatures, yielding a correspondence between m_h^2 and v/ϕ , which we can plug into the full Higgs potential as $m_h^2(\phi)$. The results for VEV and Higgs mass are shown in figure 3.7

It should be noted, that small numerical errors in $m_h^2(\phi)$ can have a large impact on $m_h^2 = \left. \frac{d^2 V_{\text{eff}}}{d\phi^2} \right|_{\phi=v}$, as these errors are exacerbated both by the exponential and the second derivative. To combat this, m_h^2 and v are evaluated at 300 different points and the dataset is smoothed in a smoothing spline with smoothing parameter $\lambda_{\text{smooth}} = 1000$.

As also noted in [22], it would be more consistent to iterate the process given above multiple times, each time receiving new expressions for VEV and mass until the mass converges. However, due to the strong amplification of numerical errors in each step, this would be a challenging endeavour, which will not be pursued here.

The reader should note that a possible gauge-invariant derivation of the effective potential has recently been suggested in [87]. However, at this point, no such calculations exist for the standard model or similar scenarios. While such a calculation for the standard model would be an interesting future project, this is beyond the scope of this thesis.

The temperature dependence of the Higgs VEV also impacts all other occurring masses. As we have already seen in section 2.3, the mass of the dark matter candidate depends on the VEV

as $m_S(T) = \sqrt{\mu_S^2 + \frac{1}{2}\lambda_{hS}v^2(T)}$. On the other hand, the masses of standard model particles generally depend linearly on the VEV, allowing us to write $m_{\text{SM}}(T) = m_{\text{SM}}(0)\frac{v(T)}{v(0)}$. This allows us to scale both the masses of the dark matter, as well as the standard model particle with the Higgs VEV.

4 Numerical results

In the previous chapters, we discussed multiple analytical calculations. Many of these calculations have also been implemented numerically. For the details of the implementations, refer to appendix A.

4.1 Comparing the impact of different particle species

Since we only discussed the self energies from fermion loops in section 3.5, it makes sense to compare the numerical results from the CTP formalism only with the $2 \rightarrow 2$ fermion annihilation channel (and the decay process). For an accurate comparison, we will also reduce the decay width Γ showing up in the Breit-Wigner propagator to the decay width to the considered fermions. However, as we had seen in section 2.7, multiple other channels also contribute to the DM production.

In figure 4.1 we can see the resulting relic densities, both under considerations of all the channels described in section 2.7, as well as from only the heavy fermions. For simplicity's sake and since this is only a qualitative question, the calculations were performed in the most simple case. This means, we only considered Boltzmann statistics and no effects from the temperature dependent Higgs potential. However, even here, we can see, that the DM production is heavily dominated by the annihilation of fermions and the direct decay of the Higgs in the considered regime. The inclusion of all channels changes the resulting relic densities by about 3%, when decay is allowed. We will use this as a justification, to only consider the fermion annihilation in the following. One should keep in mind that this is not a good approximation when resonant processes are disallowed due to high dark matter masses. There, the production is dominated by vector boson annihilation.

4.2 CTP calculations and different RIS schemes

A comparison between the relic densities generated under different RIS schemes and in the CTP formalism can be seen in figure 4.2. We here ignore the effects from the temperature dependent Higgs potential and instead use an instantaneous EWSB. In figure 4.2a only the $b\bar{b}$ annihilation channel, which is the most dominant channel in this regime, is considered. Of course, this also includes the production from Higgs decay in the Boltzmann equation

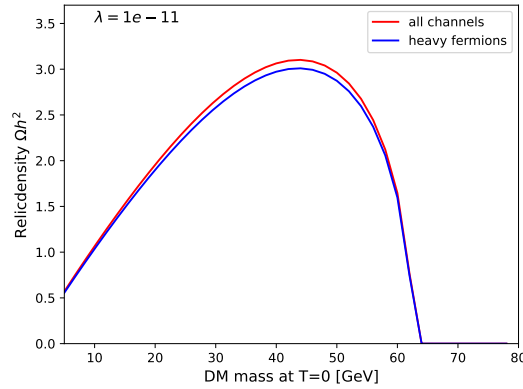


Figure 4.1: Freeze-in relic densities for different dark matter masses and coupling $\lambda = 10^{-11}$ from the semi-classical Boltzmann equation, taking into account decay processes, as well as different tree-level $2 \rightarrow 2$ processes. In one case, we consider only the annihilation of fermions, while in the other case all SM fermion annihilations are considered. Here we assumed Boltzmann statistics and a constant Higgs potential.

calculations. In figure 4.2b instead the annihilation of the four heaviest fermions t, b, c, τ are considered.

In all of the considered schemes, we can observe a qualitatively similar behaviour. The relic density shows a peak for masses of about 44 GeV. We can also see that the relic density drastically decreases for dark matter masses above $m_S = 62,5 \text{ GeV} = m_h/2$, as Higgs decays into dark matter and resonant enhancement of processes are forbidden for larger masses. The relic densities for higher masses are suppressed by an order $10^{-5} - 10^{-6}$ compared to the regime where decay is possible. The overall shape of the relic density - dark matter mass curves can be explained by looking at the shape of the relevant decay rates in equation (2.93) and crosssections in equation (2.112). Both depend on the mass of the DM as $\sqrt{s - 4m_S^2}$, with $s \leq 4m_S^2$. This leads to a larger particle density produced for smaller DM masses. At the same time the relic density depends linearly on the particle mass as seen in equation (2.34).

As expected, neglecting any RIS scheme leads to a significantly (more than 60%) higher relic density than in the CTP formalism, while the real-part scheme still yields more than 30% larger values. However, we can see that relic densities from the PVS and SRS schemes are almost identical and only slightly ($< 2\%$) larger than the results from the CTP formalism. It is expected that PVS and SRS scheme are close, as they actually converge to the same result in the narrow width approximation as mentioned in section 2.8 and [11]. The smaller relic densities appearing in the CTP formalism might be due to higher order loop-corrections such as the one appearing in section 3.6.3 and are not necessarily an effect caused by the choice of

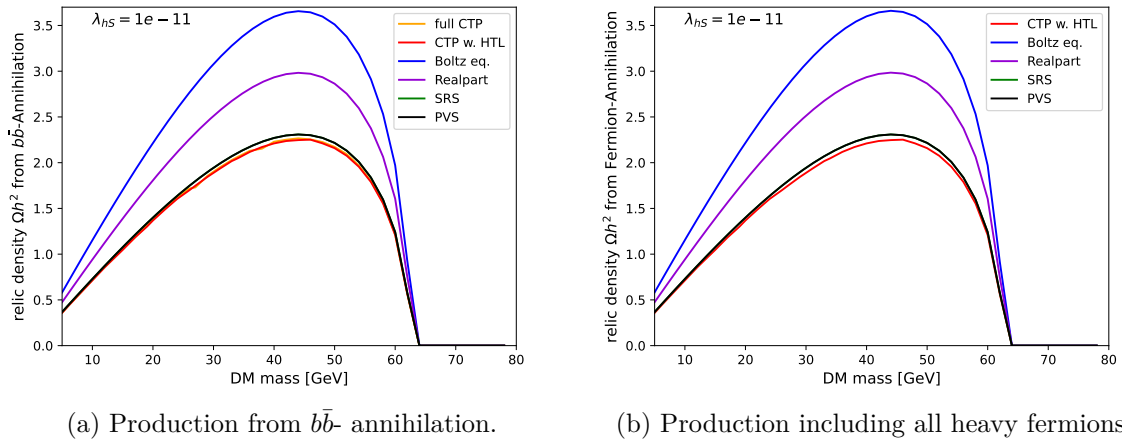


Figure 4.2: Freeze-in relic densities for different dark matter masses and coupling $\lambda = 10^{-11}$ from the semi-classical Boltzmann equation under different RIS subtraction schemes and from the KB eq. of the CTP formalism. Here, the calculations are performed for a constant Higgs potential, but full statistics are taken into account. In (a) the only $2 \rightarrow 2$ channel considered is the $b\bar{b}$ -annihilation. In (b) the three heavy quarks and the τ -lepton are considered. One should note that the relic-densities generated by the SRS scheme are not visible here, as they are (almost) identical to the ones generated by the PVS scheme.

subtraction schemes.

We can also see in figure 4.2a, that the HTL approximation of the hermitian self energy has basically no impact on the resulting relic densities. So, we will only perform the calculations with the HTL approximated hermitian self energy in the further calculations.

When we consider the annihilation of all heavy fermions (t, b, c, τ) as in figure 4.2b, we can see that the relic densities calculated from the Boltzmann equation barely differ from those calculated including only the $b\bar{b}$ annihilation channel. This makes sense, as the dark matter production is heavily dominated by decays and $b\bar{b}$ annihilation in this regime. We had already seen in figure 4.1 that the inclusion of additional channels barely impacts the relic density results. The same holds for the relic densities calculated in the CTP formalism.

4.3 Impact of the temperature dependent Higgs potential

We also performed calculations taking into account the temperature dependence of the Higgs potential as described in section 3.7. The resulting relic densities and a comparison to the relic densities in figure 4.2 can be seen in figure 4.3. Across all schemes, the inclusion of the temperature dependent Higgs potential leads to lower relic densities. This is expected, since

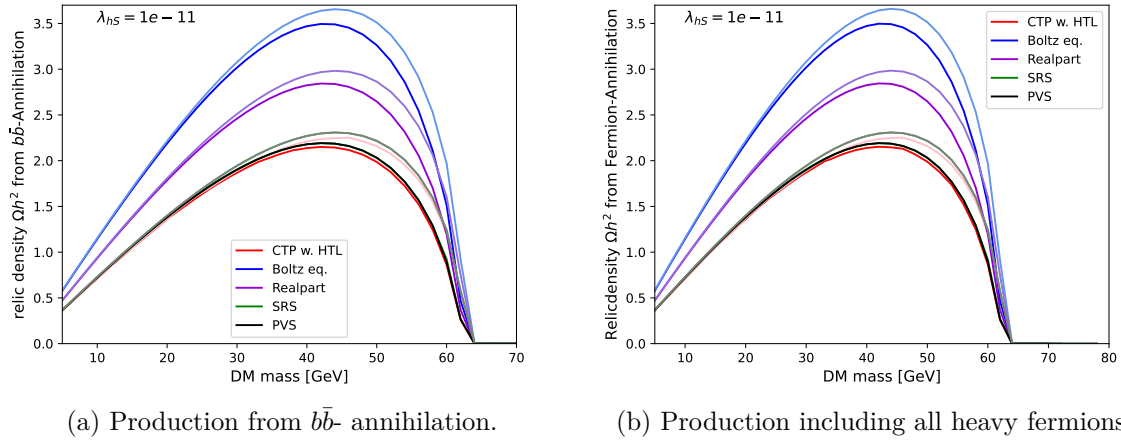


Figure 4.3: As in Figure 4.2, but considering the thermal evolution of the Higgs potential and related quantities. The relic densities derived without taking into account the temperature evolution of the Higgs potential are presented in lighter tones of the colors. As above, we cannot distinguish the results from the SRS and PVS scheme, as they are very close.

the coupling between dark matter and the standard model is proportional to the Higgs VEV which will be small at high temperatures in a temperature dependent setup.

The temperature dependent potential has the greatest impact for large dark matter masses. This is expected, since the most relevant temperature for the production is proportional to the DM mass. We find a very similar effect on the relic density independent of the calculation scheme utilised. We find a suppression of the DM relic density by about 4% at a DM mass of 40 GeV, 8% at 50 GeV and 25% at 60 GeV.

In total, we can see that the PVS and SRS schemes yield results which are fairly close to those calculated from the CTP formalism. This is consistent with the statement, that there is no RIS problem using fully resummed propagators from the CTP formalism and shows, that the SRS and PVS schemes are both consistent schemes of treating the RIS problem. We also found, that the proper treatment of the temperature dependent Higgs potential has a more significant impact on the relic density calculations than the choice of RIS subtraction scheme. As long as the scheme is chosen from SRS, PVS or calculations in the CTP formalism.

5 Conclusion

In this thesis, we investigated the freeze-in production of dark matter. For the ease of calculation, we considered the scalar singlet model of dark matter. This is a very simple model which still shows some interesting phenomena. As we had seen in the first part of the thesis, the standard procedure is based on the semi-classical Boltzmann equation. This equation does not naturally account for temperature dependent effects and exhibits a double-counting problem when real intermediate particle states are involved in the production. In order to properly deal with these problems, we used thermal field theory, more specifically the closed time path formalism. We saw that the Kadanoff-Baym equations yield a replacement for the Boltzmann equation, which naturally accounts for RIS and deals with some temperature dependent effects. The resulting kinetic equations relied on the DM self energy, which was subsequently calculated.

To account for the thermal evolution of Higgs VEV and mass, we also investigated the temperature dependence of the effective Higgs potential. We were able to evaluate the temperature dependent Higgs potential to one loop order, by evaluating tadpole diagrams in the CTP formalism.

We found out that the SRS and PVS schemes both present good RIS subtraction schemes and the calculated relic densities in these schemes differed by only about 2% from the results in the CTP formalism. The impact from a proper treatment of the temperature dependent Higgs potential turns out to be more significant in some scenarios, depending on the dark matter mass and the relevant temperature scales. At high masses we found an impact of 25% from the proper treatment of the temperature dependent potential.

6 Outlook

The calculations in the scalar singlet model were especially easy, since only the Higgs portal is available for the production of dark matter. This in particular means that there is no mixing of different channels. In a scenario where multiple mixing channels exist (e.g., in a model with a scalar mediator m mixing with the Higgs h), the RIS schemes break down,

since they are defined on the squared propagator.

It is interesting to note that a consistent description is in principle possible in the CTP formalism. This would require the introduction of additional effective propagators, connecting different particle species (e.g., h and mediator m). The Dyson-Schwinger equation (3.54) uniquely determines the construction, but the equations for resummed propagators are difficult to solve in practice. A similar approach was taken in [88], to account for fermion flavour changing processes in the Matsubara formalism. However, only 1-loop propagators in the Matsubara formalism are considered there. It would be interesting to find expressions for resummed species changing propagators in the CTP formalism to extend the method described in this thesis to such models where a mixing of mediators appears. This is especially interesting, as traditional RIS schemes are not applicable in these cases.

In our discussion regarding the temperature dependent Higgs potential, we already mentioned a couple of potential problems with the procedure. As mentioned there, it would be much more consistent to use an iterative approach that improves the precision of the mass calculations in each step. We chose not to use this approach here due to numerical instability, but this could be further investigated in the future.

Additionally, some of the concerns in the description of thermal effective potentials are due to potentially gauge dependent results. Recently, there has been a proposal for the construction of gauge independent effective potentials in [87]. Extending their proposal to realistic models, such as the standard model and adjacent theories could alleviate some of the concerns of gauge dependence.

In a medium or at high temperatures the dynamics of fermion loops, as in the dark matter self energy in this thesis, can be influenced by additional gauge boson scatterings. Including full ladder diagrams and their different interference terms can lead to leading order correction to the scattering rates and the resulting dark matter densities. This is the so-called Landau-Pomeranchuk-Migdal (LPM) effect.

The predictions of this thesis could be improved by the inclusion of the LPM effect. A consistent implementation of the LPM effect into calculations from thermal field theory was very recently presented in [89]. There, an impact on the relic density of up to 27% was reported. While [89] used a different dark matter model for their calculations, a significant impact is also expected in the scalar singlet model.

A Notes about the numerical implementation

A.1 Solving the semi-classical Boltzmann equation in Python

The numerical solution of the semi-classical Boltzmann equation of chapter 2 was performed in Python. To do so, the evolution equations were cast into the form of equation (2.32) and solved by applying the `scipy.integrate.solve_ivp` function using an implicit method based on the backward differentiation formula (BDF). The solution of the DM density evolution was performed assuming an initially vanishing density $n_{DM} = Y_{DM} = 0$ at EWSB, which was set to 150,2 GeV based on the evolution of the Higgs potential described in section 3.7. The evolution was performed down to temperatures of 5 GeV, before the relic density was calculated indicated as in equation (2.34).

The occurring integrals on the RHS of the differential equation were also solved using `scipy.integrate` by applying the `quad` function. Since the $K_1(x)$ Besselfunctions appearing in the equations under the assumption of Boltzmann statistics show numerically complicated behaviour for small values of x , we choose an approximation, as in [62]. The modified Besselfunction of the second kind and first degree $K_1(x)$ as in equation (2.46) can be written for $x < 2$ as:

$$K_1(x) = (\log(x/2)I_1(x)) + (1/x)(1 + y(0.15443144 + y(-0.67278579 + y(-0.18156897 + y(-0.1919402e - 1 + y(-0.110404e - 2 + y(-0.4686e - 4))))))) \quad (\text{A.1})$$

Here, $I_1(x)$ is the modified Besselfunction of order 1 and $y = x^2/4$.

Additionally, there are multiple QCD values, such as the Quark masses or the strong coupling constant α_s appearing in the calculations. These QCD values depend quite strongly on the energy scale. We take this dependence into account to 4-loop order as in [90]. The masses and couplings are then evaluated at the scale of the dark matter mass m_s where the most relevant processes are expected to take place.

To keep the results calculated from the semi-classical Boltzmann equation comparable to the ones received from the CTP formalism, the widths of the Higgs showing up in the calculations (e.g., in equation (2.112)), are taken to be just the decay widths into the annihilating particle species. This is done, since in the CTP formalism both annihilations as well as widths are determined by the loop particles.

A.2 FTFT calculations in C

For reasons of performance, the numerical evaluation of the equations from thermal field theory is done in C, using also the university's high performance cluster PALMA II. Most occurring integrals were performed using the GSL [91] Integration routines *qag* or *cquad*, being adaptive and doubly-adaptive integration routines based on the quadrature rule. An exception is the 2-dimensional integral showing up in equation (3.89), which is calculated using the *Cuhre* method of the Cuba [92] library.

To use the computational resources of the PALMA II cluster effectively, we calculated a 100×100 point grid in momentum and temperature of the DM self energy occurring in equation (3.89). This grid is interpolated over using the GSL *interp2d* function performing a bicubic interpolation. This allows to perform the remaining momentum integral and solve the differential equation in equation (3.80) using the GSL *odeiv2* class with an explicit Adams-Bashforth and implicit Adams-Moulton predictor-corrector method.

The scale dependence of QCD values is taken into account precisely as in the semi-classical case above.

A.3 Calculation of the Higgs VEV and mass in Python

We also calculated and tabulated the temperature dependent Higgs VEV and mass, to use in the other numerical implementations. The calculations were performed in Python, as performance was not critical.

The potential was written as described in section 3.7 and the occurring integrals were solved using the *scipy.integrate.quad* function as in the calculation in the Boltzmann equation formalism. The potential was minimized using the *scipy.optimize.minimize* function employing a Broyden-Fletcher-Goldfarb-Shanno algorithm. To find the mass of the Higgs, the second derivative of the potential was calculated at its minimum using the *scipy.differentiate.hessian* function which is based on the finite difference formula of order 8.

As mentioned in section 3.7, we first evaluated the Higgs properties without taking into account the self interaction of the Higgs. The result was used as an ansatz of the field dependent mass of the Higgs. To eliminate numerical discontinuities the discrete values of mass and VEV were related using the *scipy.interpolate.make_smoothing_spline* function which provides a linear regression with an additional weight based on the second derivative of the spline function. The resulting mass function $m_h(\phi)$ was plucked into the full version of

the Higgs potential.

B Higgs potential in high temperature approximation

We will here use a simple way to construct the effective potential, which relies on a high temperature approximation, which allows us to receive analytic solutions. The procedure is based on [84], but turns out to be not well suited for our purpose.

If we only consider effects from the top quark, vector bosons and the Higgs as in section 3.7, the 1-loop thermal correction of the Higgs potential is in high temperature expansion:

$$V_1(\phi) = \frac{T^2}{32}(8\lambda + 4y_t^2 + 3g^2 + g'^2)\phi^2 \quad (\text{B.1})$$

And we can write the complete leading order potential as:

$$V_{LO} = \frac{1}{2}(-m^2 + \frac{T^2}{16}(8\lambda + 4y_t^2 + 3g^2 + g'^2))\phi^2 + \frac{1}{4}\lambda\phi^4 \quad (\text{B.2})$$

We can directly calculate the minimum of this potential and receive the VEV as

$$\phi_{min}^2 = \frac{1}{\lambda}(m^2 - \frac{T^2}{16}(8\lambda + 4y_t^2 + 3g^2 + g'^2)) \quad (\text{B.3})$$

As this is the leading order result, one might consider to use the tree-level expression for the mass of the Higgs. Then it is $m_h^2 = 3\lambda v^2 - m^2$, which here turns into:

$$m_h^2 = 2m^2 - \frac{3T^2}{16}(8\lambda + 4y_t^2 + 3g^2 + g'^2) \quad (\text{B.4})$$

As we can see in figure B.1, there are significant differences between the high temperature and the full result. The results differ both for the vev and for the mass of the Higgs. We can see that the numerical evaluation of the Higgs mass (taking a second derivative of the potential) is closer than the analytical to the results from the full calculation. This is because the self energy effects (such as Π^H in earlier parts of the thesis) which would further modify the mass, are ignored in the analytical mass calculation. The differences to the full results occur on all temperature scales, which are relevant for the analysis in this thesis, making the high temperature approximation ill suited for the calculations here.

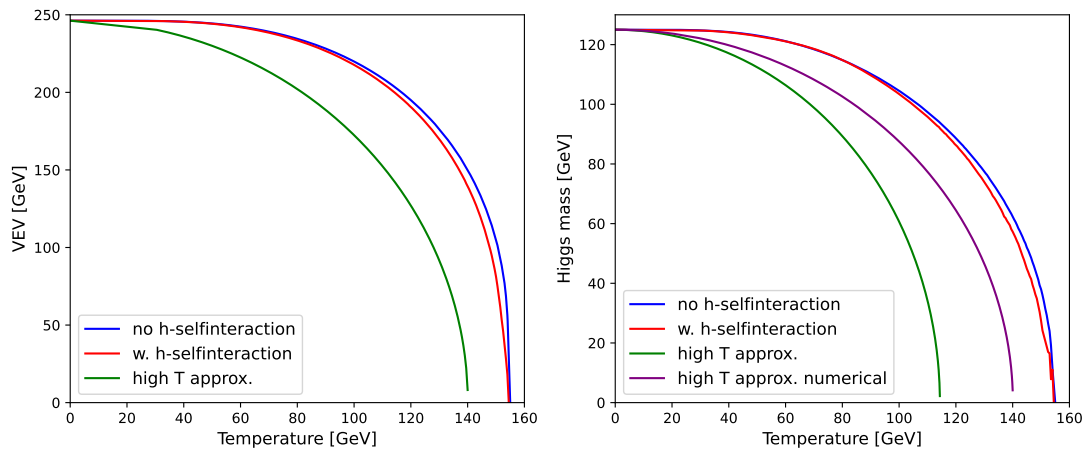


Figure B.1: As in figure 3.7, but added are the analytical results from the high temperature approximation (in green) and the numerical differentiation of the high temperature potential (in purple). We can see, that there is a significant difference between the high T approximation and the full calculation employed in section 3.7.

Bibliography

- [1] S.M. Carroll, The Cosmological constant, Living Rev. Rel. **4** (2001) 1 [astro-ph/0004075].
- [2] P. Bull et al., Beyond Λ CDM: Problems, solutions, and the road ahead, Phys. Dark Univ. **12** (2016) 56 [1512.05356].
- [3] PLANCK collaboration, Planck 2018 results. VI. Cosmological parameters, Astron. Astrophys. **641** (2020) A6 [1807.06209].
- [4] EBOSS collaboration, Completed sdss-iv extended baryon oscillation spectroscopic survey: Cosmological implications from two decades of spectroscopic surveys at the apache point observatory, Phys. Rev. D **103** (2021) 083533 [2007.08991].
- [5] M. Cirelli, A. Strumia and J. Zupan, Dark Matter, 2406.01705.
- [6] P. Gondolo and G. Gelmini, Cosmic abundances of stable particles: Improved analysis, Nuclear Physics B **360** (1991) 145.
- [7] A. Poulin, Dark matter freeze-out in modified cosmological scenarios, Phys. Rev. D **100** (2019) 043022.
- [8] E.W. Kolb and M.S. Turner, The Early Universe, vol. 69, Taylor and Francis (5, 2019), 10.1201/9780429492860.
- [9] G.B. Gelmini, The hunt for dark matter., in Theoretical Advanced Study Institute in Elementary Particle Physics: Journeys Through the Precision Frontier: Amplitudes for Colliders, pp. 559–616, 2015, DOI [1502.01320].
- [10] T. Bringmann, S. Heeba, F. Kahlhoefer and K. Vangsnes, Freezing-in a hot bath: resonances, medium effects and phase transitions, JHEP **02** (2022) 110 [2111.14871].
- [11] K. Ala-Mattinen, M. Heikinheimo, K. Tuominen and K. Kainulainen, Anatomy of real intermediate state-subtraction scheme, Phys. Rev. D **108** (2023) 096034 [2309.16615].
- [12] P. Maták, Unitarity, real-intermediate states, and fixed-order approach to resonant dark matter annihilation, Phys. Rev. D **109** (2024) 043008.

- [13] M. Becker, E. Copello, J. Harz and C. Tamarit, Dark matter freeze-in from non-equilibrium qft: towards a consistent treatment of thermal effects, 2312.17246.
- [14] L.P. Wiggering, Precise Theoretical Predictions for the Dark Matter Relic Density and Neutrino Dynamics in the Early Universe, Ph.D. thesis, Munster U., 2024.
- [15] T. Matsubara, A New approach to quantum statistical mechanics, Prog. Theor. Phys. **14** (1955) 351.
- [16] N. Haque, Finite temperature qcd four-point function in the presence of a weak magnetic field within the hard thermal loop approximation, Phys. Rev. D **96** (2017) 014019.
- [17] W. Alberico, A. Beraudo, P. Czerski and A. Molinari, Finite momentum meson correlation functions in a qcd plasma, Nuclear Physics A **775** (2006) 188.
- [18] M.L. Bellac, Thermal Field Theory, Cambridge Monographs on Mathematical Physics, Cambridge University Press (3, 2011), 10.1017/CBO9780511721700.
- [19] F.D. Villalba-Pardo and C.J. Quimbay, Neutrino dispersion relations at finite temperature and density in the left-right symmetric model, 1004.1074.
- [20] M. Drewes, Y. Georis, M. Klasen, L.P. Wiggering and Y.Y.Y. Wong, Towards a precision calculation of n_{eff} in the standard model. part iii. improved estimate of nlo contributions to the collision integral, JCAP **06** (2024) 032 [2402.18481].
- [21] M. Quiros, Finite temperature field theory and phase transitions, in ICTP Summer School in High-Energy Physics and Cosmology, pp. 187–259, 1, 1999 [hep-ph/9901312].
- [22] P. Bittar, S. Roy and C.E.M. Wagner, Self consistent thermal resummation: A case study of the phase transition in 2hdm, Arxiv:2504.02024v1.
- [23] Z. Si, H. Wang, L. Wang, Y. Xiao and Y. Zhang, The bubble wall velocity in local thermal equilibrium with full effective potential, 2505.19584.
- [24] C.E. Yaguna, The Singlet Scalar as FIMP Dark Matter, JHEP **08** (2011) 060 [1105.1654].
- [25] G. Bertone and D. Hooper, History of dark matter, Rev. Mod. Phys. **90** (2018) 045002.
- [26] J.H. Oort, The force exerted by the stellar system in the direction perpendicular to the galactic plane and some related problems, Bulletin of the Astronomical Institutes of the Netherlands **6** (1932) 249.

- [27] J.I. Read, The local dark matter density, Journal of Physics G: Nuclear and Particle Physics **41** (2014) 063101.
- [28] P. Salucci, The distribution of dark matter in galaxies, Astron. Astrophys. Rev. **27** (2019) 2 [1811.08843].
- [29] A.H. Nelson and P.R. Williams, Recent observations of the rotation of distant galaxies and the implication for dark matter, Astron. Astrophys. **687** (2024) A261 [2401.13783].
- [30] F. Zwicky, Die Rotverschiebung von extragalaktischen Nebeln, Helv. Phys. Acta **6** (1933) 110.
- [31] F. Zwicky, On the Masses of Nebulae and of Clusters of Nebulae, Astrophys. J. **86** (1937) 217.
- [32] J.M. Kubo, A. Stebbins, J. Annis, I.P. Dell'Antonio, H. Lin, H. Khiabanian et al., The Mass Of The Coma Cluster From Weak Lensing In The Sloan Digital Sky Survey, Astrophys. J. **671** (2007) 1466 [0709.0506].
- [33] EROS collaboration, Not enough stellar mass machos in the galactic halo, Astron. Astrophys. **355** (2000) L39 [astro-ph/0002253].
- [34] D. Clowe, M. Bradač, A.H. Gonzalez, M. Markevitch, S.W. Randall, C. Jones et al., A direct empirical proof of the existence of dark matter*, The Astrophysical Journal **648** (2006) L109.
- [35] T. Baker et al., Novel Probes Project: Tests of gravity on astrophysical scales, Rev. Mod. Phys. **93** (2021) 015003 [1908.03430].
- [36] S.S. McGaugh, A tale of two paradigms: the mutual incommensurability of λ cdm and mond, Can. J. Phys. **93** (2015) 250 [1404.7525].
- [37] H.-Y. Schive, T. Chiueh and T. Broadhurst, Cosmic structure as the quantum interference of a coherent dark wave, Nature Phys. **10** (2014) 496 [1406.6586].
- [38] A. Pozo et al., Galaxy formation with wave/fuzzy dark matter: The core-halo structure, 2310.12217.
- [39] G. Jungman, M. Kamionkowski and K. Griest, Supersymmetric dark matter, Physics Reports **267** (1996) 195.

- [40] L. Roszkowski, E.M. Sessolo and S. Trojanowski, Wimp dark matter candidates and searches—current status and future prospects, Reports on Progress in Physics **81** (2018) 066201.
- [41] XENON collaboration, First dark matter search with nuclear recoils from the xenonnT experiment, Phys. Rev. Lett. **131** (2023) 041003.
- [42] N. Bernal, M. Heikinheimo, T. Tenkanen, K. Tuominen and V. Vaskonen, The Dawn of FIMP Dark Matter: A Review of Models and Constraints, Int. J. Mod. Phys. A **32** (2017) 1730023 [1706.07442].
- [43] L.J. Hall, K. Jedamzik, J. March-Russell and S.M. West, Freeze-in production of fimp dark matter, Journal of High Energy Physics **2010** (2010) .
- [44] M. Blennow, E. Fernandez-Martinez and B. Zaldivar, Freeze-in through portals, JCAP **01** (2014) 003 [1309.7348].
- [45] E. Frangipane, S. Gori and B. Shakya, Dark matter freeze-in with a heavy mediator: beyond the eft approach, Journal of High Energy Physics **2022** (2022) .
- [46] J. McDonald, Thermally generated gauge singlet scalars as selfinteracting dark matter, Phys. Rev. Lett. **88** (2002) 091304 [hep-ph/0106249].
- [47] M. Frigerio, T. Hambye and E. Masso, Sub-gev dark matter as pseudo-goldstone from the seesaw scale, Phys. Rev. X **1** (2011) 021026 [1107.4564].
- [48] N. Chakrabarty, P. Konar, R. Roshan and and S. Show, Thermally corrected masses and freeze-in dark matter: A case study, Phys. Rev. D **107** (2023) 035021 [2206.02233].
- [49] K.G. Vangsnes, Freeze-in production of scalar singlet dark matter, Master's thesis, UNIVERSITY OF OSLO, 2021.
- [50] K. Ala-Mattinen and K. Kainulainen, Precision calculations of dark matter relic abundance, JCAP **09** (2020) 040 [1912.02870].
- [51] C. Burgess, M. Pospelov and T. ter Veldhuis, The minimal model of nonbaryonic dark matter: a singlet scalar, Nuclear Physics B **619** (2001) 709–728.
- [52] Y. Yu, T.-P. Tang and L. Feng, New constraints on singlet scalar dark matter model with lz, invisible higgs decay and gamma-ray line observations, Nucl. Phys. B **1015** (2025) 116910 [2410.21089].

- [53] J.M. Cline, P. Scott, K. Kainulainen and C. Weniger, Update on scalar singlet dark matter, Physical Review D **88** (2013) .
- [54] O.F. Piattella, Lecture Notes in Cosmology, UNITEXT for Physics, Springer, Cham (2018), 10.1007/978-3-319-95570-4, [1803.00070].
- [55] A. Friedmann, On the Possibility of a world with constant negative curvature of space, Z. Phys. **21** (1924) 326.
- [56] A. Aboubrahim, M. Klasen and L.P. Wiggering, Forbidden dark matter annihilation into leptons with full collision terms, Journal of Cosmology and Astroparticle Physics **2023** (2023) 075.
- [57] M. Drees, F. Hajkarim and E.R. Schmitz, The effects of qcd equation of state on the relic density of wimp dark matter, Journal of Cosmology and Astroparticle Physics **2015** (2015) 025.
- [58] M.E. Peskin and D.V. Schroeder, An Introduction to quantum field theory, Addison-Wesley, Reading, USA (1995), 10.1201/9780429503559.
- [59] S. Weinberg, The Quantum theory of fields. Vol. 1: Foundations, Cambridge University Press (6, 2005), 10.1017/CBO9781139644167.
- [60] M. Cannoni, Lorentz invariant relative velocity and relativistic binary collisions, Int. J. Mod. Phys. A **32** (2017) 1730002 [1605.00569].
- [61] M.D. Schwartz, Quantum Field Theory and the Standard Model, Cambridge University Press (3, 2014).
- [62] G. Alguero, G. Belanger, F. Boudjema, S. Chakraborti, A. Goudelis, S. Kraml et al., micrOMEGAs 6.0: N-component dark matter, Comput. Phys. Commun. **299** (2024) 109133 [2312.14894].
- [63] W.R. Inc., “Mathematica, Version 14.2.” <https://www.wolfram.com/mathematica>.
- [64] E.W. Kolb and S. Wolfram, Baryon number generation in the early universe, Nuclear Physics B **172** (1980) 224.
- [65] J.N. Fry, K.A. Olive and M.S. Turner, Evolution of cosmological baryon asymmetries. i. the role of gauge bosons, Phys. Rev. D **22** (1980) 2953.
- [66] M. Beneke, B. Garbrecht, M. Herranen and P. Schwaller, Finite number density corrections to leptogenesis, Nuclear Physics B **838** (2010) 1–27.

- [67] W. Buchmüller, P. Di Bari and M. Plümacher, Leptogenesis for pedestrians, Annals of Physics **315** (2005) 305–351.
- [68] K. Ala-Mattinen, M. Heikinheimo, K. Kainulainen and K. Tuominen, Momentum distributions of cosmic relics: Improved analysis, Phys. Rev. D **105** (2022) 123005 [2201.06456].
- [69] G. Bélanger, F. Boudjema, A. Goudelis, A. Pukhov and B. Zaldivar, micrOMEGAs5.0 : Freeze-in, Comput. Phys. Commun. **231** (2018) 173 [1801.03509].
- [70] N. Landsman and C. van Weert, Real- and imaginary-time field theory at finite temperature and density, Physics Reports **145** (1987) 141.
- [71] L.V. Keldysh, Diagram technique for nonequilibrium processes, Zh. Eksp. Teor. Fiz. **47** (1964) 1515.
- [72] J.S. Schwinger, Brownian motion of a quantum oscillator, J. Math. Phys. **2** (1961) 407.
- [73] Y. Takahashi and H. Umezawa, Thermo field dynamics, Collect. Phenom. **2** (1975) 55.
- [74] Y. Takahashi and H. Umezawa, Thermo field dynamics, Int. J. Mod. Phys. B **10** (1996) 1755.
- [75] H. Matsumoto, Y. Nakano and H. Umezawa, An equivalence class of quantum field theories at finite temperature, J. Math. Phys. **25** (1984) 3076.
- [76] T. Altherr and D. Seibert, Problems of perturbation series in non-equilibrium quantum field theories, Physics Letters B **333** (1994) 149–152.
- [77] K.-c. Chou, Z.-b. Su, B.-l. Hao and L. Yu, Equilibrium and nonequilibrium formalisms made unified, Phys. Rept. **118** (1985) 1.
- [78] H. Matsumoto, I. Ojima and H. Umezawa, Perturbation and renormalization in thermo field dynamics, Annals Phys. **152** (1984) 348.
- [79] H.J. Groenewold, On the Principles of elementary quantum mechanics, Physica **12** (1946) 405.
- [80] E. Braaten and R.D. Pisarski, Soft amplitudes in hot gauge theories: A general analysis, Nucl. Phys. B **337** (1990) 569.
- [81] P. Elmfors, K. Enqvist and I. Vilja, Thermalization of the higgs field at the electroweak phase transition, Nucl. Phys. B **412** (1994) 459 [hep-ph/9307210].

- [82] J. Löfgren, Stop comparing resummation methods, J. Phys. G **50** (2023) 125008 [2301.05197].
- [83] H.H. Patel and M.J. Ramsey-Musolf, Baryon washout, electroweak phase transition, and perturbation theory, JHEP **07** (2011) 029 [1101.4665].
- [84] A. Ekstedt and J. Löfgren, A Critical Look at the Electroweak Phase Transition, JHEP **12** (2020) 136 [2006.12614].
- [85] H. Patel, “Uses and abuses of the coleman-weinberg effective potential.” Talk at MPI-K: https://www.mpi-hd.mpg.de/lin/seminar_theory/talks/Talk_Patel_270114.pdf, 2014.
- [86] M. Garny and T. Konstandin, On the gauge dependence of vacuum transitions at finite temperature, JHEP **07** (2012) 189 [1205.3392].
- [87] D. Balui, J. Chakraborty, D. Dey and S. Mohanty, Gauge invariant effective potential, Phys. Rev. D **111** (2025) 085032 [2502.17156].
- [88] A. Hataei and S.S. Gousheh, Thermal fermion propagators and flavor-changing via loop corrections in the early universe, Arxiv:2504.01150v1.
- [89] M. Becker, M.J.F. Lozano, J. Harz and C. Tamarit, Multiple soft scatterings in scalar dark matter freeze-in, 2506.11185.
- [90] K.G. Chetyrkin, J.H. Kuhn and M. Steinhauser, Rundec: A mathematica package for running and decoupling of the strong coupling and quark masses, Comput. Phys. Commun. **133** (2000) 43 [hep-ph/0004189].
- [91] M.C. Galassi, J. Davies, J. Theiler, B. Gough, G. Jungman, P. Alken et al., GNU Scientific Library, Network Theory, Ltd. (8, 2019).
- [92] T. Hahn, CUBA: A Library for multidimensional numerical integration, Comput. Phys. Commun. **168** (2005) 78 [hep-ph/0404043].